AGU ADVANCING EARTH AND SPACE SCIENCES

Earth's Future

RESEARCH ARTICLE
10.1029/2024EF005580

# Quantifying $CO_2$ and Non-$CO_2$ Contributions to Climate Change Under 1.5°C and 2°C Adaptive Emission Scenarios

**Donghyun Lee[1,2], Sarah N. Sparrow[3], Matteo Willeit[4], Paulo Ceppi[1], and Myles R. Allen[2,5]**

[1]Department of Physics, Imperial College London, London, UK, [2]School of Geography and the Environment, University of Oxford, Oxford, UK, [3]Department of Engineering Science, University of Oxford, Oxford, UK, [4]Potsdam Institute for Climate Impact Research (PIK), Member of the Leibniz Association, Potsdam, Germany, [5]Department of Physics, University of Oxford, Oxford, UK

**Key Points:**

- We assess uncertainty in temperature and precipitation change in perturbed-physics ensembles for 1.5°C and 2°C adaptive emission scenarios
- For a given warming level and non-$CO_2$ emissions scenario, aerosol forcing dominates uncertainty in the carbon budget and climate response
- Regional precipitation impacts of $CO_2$ forcing are robust, highlighting the need for rapid $CO_2$ emission mitigation

**Supporting Information:**

Supporting Information may be found in the online version of this article.

**Correspondence to:**

D. Lee,
donghyun.lee@imperial.ac.uk

**Citation:**

Lee, D., Sparrow, S. N., Willeit, M., Ceppi, P., & Allen, M. R. (2025). Quantifying $CO_2$ and non-$CO_2$ contributions to climate change under 1.5°C and 2°C adaptive emission scenarios. *Earth's Future*, *13*, e2024EF005580. https://doi.org/10.1029/2024EF005580

Received 1 NOV 2024
Accepted 10 MAR 2025

**Author Contributions:**

**Conceptualization:** Donghyun Lee, Sarah N. Sparrow, Myles R. Allen
**Data curation:** Donghyun Lee
**Formal analysis:** Donghyun Lee, Sarah N. Sparrow
**Funding acquisition:** Myles R. Allen
**Investigation:** Donghyun Lee, Myles R. Allen
**Methodology:** Donghyun Lee, Sarah N. Sparrow, Matteo Willeit, Myles R. Allen
**Project administration:** Myles R. Allen
**Resources:** Donghyun Lee, Sarah N. Sparrow
**Software:** Donghyun Lee, Sarah N. Sparrow, Matteo Willeit
**Supervision:** Sarah N. Sparrow, Myles R. Allen



**Abstract** The individual contributions of various human-induced forcings under scenarios compatible with the Paris Agreement targets are highly uncertain. To quantify this uncertainty, we analyze three types of models with physical parameter perturbed large ensembles under global warming levels of 1.5 and 2.0°C. The scenarios use adaptive $CO_2$ emissions, while non-$CO_2$ emissions are prescribed. The residual emission budgets in the scenarios are measured in terms of $CO_2$ forcing equivalent ($CO_2$-fe). Our simulations quantify approximately 0.8 (0.2–1.3 for a 90% confidence interval) and 1.9 (0.9–3.0) $TtCO_2$-fe for the 1.5 and 2.0°C targets by the end of the 21st century. About 37.5% (73.7%) of the budget for 1.5°C (2.0°C) originates from the $CO_2$ emission pathways, highlighting the importance of non-$CO_2$ forcings. Aerosols dominate the uncertainty in non-$CO_2$ contributions to global responses in both temperature and precipitation. Our modeling results underline the need to constrain the response to each climate forcing, particularly aerosol, to build an accurate mitigation and adaptation plan under the pledges of the Paris Agreement. Moreover, we demonstrate robust differences in global and regional temperature and precipitation responses between the higher and lower $CO_2$ emission scenarios, highlighting the significance of carbon neutrality.

**Plain Language Summary** In 2020, human activities caused global warming to reach 1.2°C since pre-industrial times, leaving us with 0.3 and 0.8°C to meet the objectives of the Paris Agreement. Multiple model simulations are conducted under the adaptive emission scenarios to explore the relevant mitigation pathways, similar to the United Nations Framework Convention on Climate Change (UNFCCC) strategy. The effects of $CO_2$ and non-$CO_2$ factors (like non-$CO_2$ greenhouse gases and aerosols) are analyzed through extensive ensemble simulations with various climate sensitivities. Our simulations illustrate that both forcing contributions are substantial, and the uncertainty in climate response to aerosols is the key hindrance to accurate climate projections under the Paris Agreement targets. The climate simulations exposed to the additional $CO_2$ emissions display substantial and measurable global and regional differences in temperature and precipitation. For example, according to the ensemble-averaged results, 1.1 trillion tons of additional $CO_2$ emissions correspond to 0.5°C and 0.7% increases in global mean temperature and precipitation, highlighting the urgency to achieve carbon emission neutrality as soon as possible. Our findings accentuate that any further $CO_2$ emission in the future increases the chance of the emergence of unfavorable climate characteristics jeopardizing current ecosystems and human well-being.

## 1. Introduction

The Paris Agreement (Paris Agreement, 2015) is a binding international agreement that aims to limit global warming to below 2.0°C while striving to keep it below 1.5°C. It is vital for mitigating the impacts of rising temperatures on our planet (e.g., Baker et al., 2018; Farinosi et al., 2020; D. Lee et al., 2018; Lehner et al., 2017; Park et al., 2022; X. Zhang et al., 2023).

Two scientific inquiries arose at the initial stage of the Paris Agreement. The first one is the definition of global warming levels to build accurate pledges. As global warming physically derives from increased radiative forcing by changing atmospheric composition with human activities, the metric of anthropogenic radiative forcing induced temperature is devised (e.g., Haustein et al., 2017; Otto et al., 2015). The other inquiry quantifies the allowable emission amount compatible with the Paris Agreement temperature goals. A simple method was suggested based on the concept of Transient Climate Response to Cumulative Emissions (TCRE, °C/$TtCO_2$)

**Validation:** Donghyun Lee, Matteo Willeit
**Visualization:** Donghyun Lee, Paulo Ceppi, Myles R. Allen
**Writing – original draft:** Donghyun Lee, Matteo Willeit, Paulo Ceppi
**Writing – review & editing:** Donghyun Lee, Matteo Willeit, Paulo Ceppi

exhibiting quasi-linearity between accumulated $CO_2$ emission amount and global mean temperature responses, explained by the relationship between thermal sensitivity and carbon cycle characteristics (Allen et al., 2009).

As forcing agents other than $CO_2$ (hereafter non-$CO_2$) may occupy the residual emission budget of $CO_2$ (Matthews et al., 2020; Millar et al., 2017; Nicholls et al., 2020), this $CO_2$ TCRE concept was updated to include the non-$CO_2$ impact by converting non-$CO_2$ emissions to comparable $CO_2$ emissions, named $CO_2$ forcing equivalent ($CO_2$-fe) emissions. The quasi-linearity between accumulated $CO_2$-fe emission amount and global-mean temperature ($CO_2$-fe TCRE, °C/Tt$CO_2$) is exploited to assess plausible ranges of the emission budget (Jenkins et al., 2018, 2021).

Although the science of emission budgets has gradually improved, gaps remain in terms of quantifying and understanding climate change impacts at the target warming levels of the Paris Agreement. Previous literature has addressed this question by examining two different types of simulation: (a) preexisting simulations from the Coupled Model Intercomparison Project (CMIP) future projection scenarios (Meinshausen et al., 2011, 2020), sampled in decades where global warming is at the chosen levels (e.g., Farinosi et al., 2020; King et al., 2018; S.-M. Lee & Min, 2018; Seneviratne & Hauser, 2020; W. Zhang & Zhou, 2021; X. Zhang et al., 2023), or (b) newly introduced simulations making assumptions about the mitigated forcing conditions (e.g., Jahn, 2018; D. Lee et al., 2018; Lehner et al., 2017; Lo et al., 2019; Madakumbura et al., 2019; Park et al., 2022; Wehner et al., 2018; W. Zhang & Zhou, 2021). The global warming impacts of 1.5°C and 2.0°C were assessed based on both types of simulations (IPCC, 2018).

However, the above approaches come with important shortcomings. The first simulation type is not forced by stabilized $CO_2$ emissions, resulting in a remaining warming trend (e.g., S.-M. Lee & Min, 2018; W. Zhang & Zhou, 2021). For the second simulation type, rough assumptions and the prescribed mitigation forcing conditions are applied for two experiments: multiple atmosphere-only models with statistical assumptions in the ocean and mitigated forcings (Lo et al., 2019; Mitchell et al., 2017) and a single climate model in an empirical mitigation scenario (Graff et al., 2019; Sanderson et al., 2017; Sigmond et al., 2018). Each experiment has a limitation: it cannot account for interactions between ocean and atmosphere or the large structural model uncertainties underlying climate projections.

More refined experiments are therefore needed to understand the remaining uncertainty in the mitigation pathways and the associated impacts on global and regional climate change. Recent work (Terhaar et al., 2022) has introduced the Adaptive Emission Reduction Approach (AERA) algorithm, which is comparable to the actual political stocktake plans of the United Nations Framework Convention on Climate Change (Català & Wyns, 2022). This algorithm creates adaptive emission scenarios based on the concept of $CO_2$-fe TCRE, simultaneously considering anthropogenic global warming levels and climate sensitivities in the thermal and carbon cycles.

AERA experiments have been performed by the Earth System Model (ESM) modeling groups (Silvy et al., 2024). However, the high computational expense of ESMs limits the number of ensembles involved and the range of possible thermal, carbon, and hydrological sensitivities considered. Comparing AERA-based projections across much larger ensembles is required to account for the extensive uncertainty exceeding the ensemble numbers of existing ESMs. These ensembles must have less complexity in model structure to save computational cost but act like ESMs in global mean senses.

To address this gap, here we quantify the forcing-driven contributions and corresponding climate responses under 1.5° and 2.0°C adaptive emission scenarios, by exploring low-cost multiple-ensemble simulations from three types of climate models at various levels of complexity but acting like ESMs. Each forcing contribution is assessed using extensive ensemble simulations with a range of thermal, carbon, and hydrological sensitivities. The global and regional climate impacts of additional $CO_2$ emissions are also examined, and the probability of climatological shifts is evaluated for various $CO_2$-induced warming levels.

## 2. Data and Methods

### 2.1. Climate Models

We use large ensembles of perturbed physical parameters in three types of climate models, each with different complexity, to assess the consistency of our findings: a simple climate model, an atmospheric-ocean coupled

**Table 1**
*The Horizontal Resolution, Ensemble Size, Simulation Years, and Climate Sensitivity Indices of Physically Perturbed Ensembles From the Three Climate Models Are Shown*

| | FaIR | HadCM3 (HC3) | CLIMBER-X (CLX) |
|---|---|---|---|
| Horizontal Resolution | – | 3.75° × 2.5° (96 × 73) | 5° × 5° (72 × 36) |
| Ensemble Size | 5,000 | 29 | 10 |
| Simulation Years | 1850–2155 | 1881–2100 | 1750–2100 |
| TCR [°C] | *1.88* (0.47) | *2.06* (0.35) | *1.87* (0.81) |
| ECS [°C] | *3.35* (1.00) | *3.57* (1.03) | *3.81* (1.27) |
| $CO_2$ TCRE [°C/Tt$CO_2$] | *0.51* (0.18) | *0.42* (0.13) | *0.53* (0.16) |
| α [%/°C] | *2.57* (0.33) | *2.03* (0.36) | *3.14* (0.21) |
| Reference | Leach et al. (2021) | Sparrow et al. (2018) | Willeit et al. (2022) |

*Note*. TCR and ECS are estimated from FaIR or tuned-FaIR for HadCM3 and CLIMBER-X. $CO_2$ TCRE and hydrological sensitivity (α) are measured from the simulation differences between AERA2.0 and AERA1.5, except for the α of FaIR. The α of FaIR follows the CMIP6 GCMs (read Section 2.3 for details). Italics and parentheses indicate the means and standard deviations of ensembles in climate sensitivity.

General Circulation Model (GCM), and an Earth system model of intermediate complexity. In our analysis, the climate sensitivities of ensemble members are within 0.7–3.0°C, 1.4–5.8°C, 0.2–1.1°C/Tt$CO_2$, and 1.4–3.8%/°C for transient climate response (TCR), equilibrium climate sensitivity (ECS), Transient Climate Response to Emission (TCRE), and hydrological sensitivity (α), respectively. The full description of each climate model and the selection process for its physically perturbed parameter ensembles are delineated in Text S1 in Supporting Information S1.

Although the models used in this study have low resolutions with simple structures in interactions relative to the latest ESMs (Silvy et al., 2024), their climate sensitivities and responses to the forcings are comparable to their full ranges of GCMs and ESMs in CMIP5 and CMIP6 (Jones & Friedlingstein, 2020; D. Lee et al., 2023; Meehl et al., 2020; Nijsse et al., 2020), proving our climate models can illustrate possible future projection uncertainties in the latest adaptive emission scenarios. The climate sensitivity ranges within the ensembles of each model type are summarized in Table 1. Our study primarily focuses on the simulation results from 2001 to 2100, with extended simulations (2101–2155) of FaIR presented in Supporting Information S1 for discussion (Figures S1 and S5).

### 2.2. AERA Application for Concentration-Driven Models

AERA, an adaptive emission scenario algorithm, generates $CO_2$ emission mitigation pathways to regulate and stabilize global warming levels (Terhaar et al., 2022). Our AERA scenarios mostly resemble the scenario of CMIP6 Shared Socio-economic Pathways (SSP) 1–2.6 (Meinshausen et al., 2020) and emerge after the simulation year 2025, with adjustments in human-induced $CO_2$ emissions reflecting model sensitivities in thermal and carbon cycles. The other anthropogenic forcings in future projections (non-$CO_2$)—the sum of methane ($CH_4$), nitrous oxide ($N_2O$), other well-mixed greenhouse gases (owmGHGs), and aerosols—continuously solely follow the SSP1-2.6 scenario, pursuing sustainable development. Note that we adopt the definition of owmGHGs (e.g., halogenated gases: CFCs, HCFCs, HFCs, PFCs, SF6, and HFOs) from Smith et al. (2021), following the component description in the Intergovernmental Panel on Climate Change Fifth Assessment Report (IPCC, 2013).

AERA generates the emission amount for the following 5 years through two iterative processes. First, AERA calculates the anthropogenic radiative forcing-driven temperature and matches it with the cumulative $CO_2$ forcing equivalent emission amount ($CO_2$-fe) to estimate $CO_2$-fe TCRE (Jenkins et al., 2018, 2021). In AERA, $CO_2$ concentration, non-$CO_2$ radiative forcings, and globally averaged temperature are used to account for anthropogenic global warming (Terhaar et al., 2022). The non-$CO_2$ radiative forcing and its $CO_2$-fe emission amount can be estimated by implementing and inverting the carbon cycle model of FaIR (Jenkins et al., 2021). The residual emission budget required to reach the target temperature can be inversely calculated with the linearity of TCRE. Second, the climate model restarts from the last simulation year and runs under the AERA scenario for the

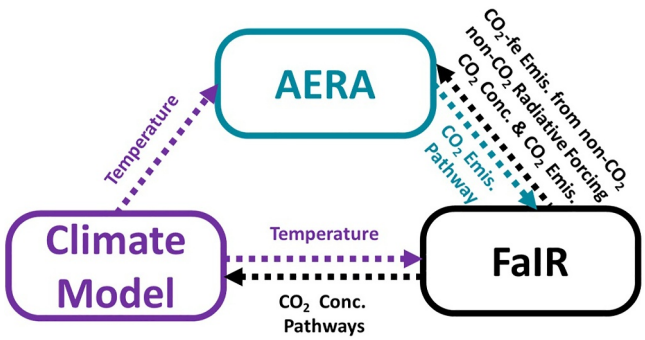


**Figure 1.** Illustration of the application of the AERA algorithm to the ESM-like simulations (FaIR, HC3F, and CLXF). Three components mutually interact every 5 years: the concentration-driven climate model, the AERA algorithm, and the emission-driven version of the FaIR model. The emission-driven version of the FaIR model translates $CO_2$ emission to concentration scenarios by considering the carbon cycle characteristics and thermal responses to the forcings. The colors represent the output variables of the climate model (purple), the AERA algorithm (turquoise), and FaIR (black). The heads of arrows denote the input direction of the variables. All the interactions between variables are globally averaged on an annual scale.

next 5 years. These two processes are repeated every 5 years (like the concept of the global stocktake framework; Català & Wyns, 2022), gradually regulating the simulated temperatures at the targeted warming level, reaching an equilibrium state eventually.

Unlike FaIR, HadCM3 (Sparrow et al., 2018) and CLIMBER-X (the early release version in Willeit et al., 2022) do not include a carbon cycle module (but note that the latest version of CLIMBER-X has a carbon cycle module; Willeit et al., 2023). To translate emissions to concentration amounts, we incorporate the carbon cycle component of FaIR to interpret the AERA $CO_2$ emission amount as comparable $CO_2$ concentrations in their projections, replacing the role of carbon cycle modules in ESMs. The AERA algorithm and FaIR are coupled with HadCM3 and CLIMBER-X every 5 years to account for carbon cycle responses in a globally averaged sense (see method details in Text S2). We denote these FaIR carbon-cycle coupled, hybrid-model results as HadCM3-FaIR (HC3F) and CLIMBER-X-FaIR (CLXF).

To investigate possible uncertainty sources in our AERA application strategy, we implemented three test experiments: (a) randomly selected carbon cycle parameters for hybrid models (Figure S1 in Supporting Information S1), (b) various options for the non-$CO_2$ pathways (Figure S5 in Supporting Information S1), and (c) definition for target $\Delta T$ (not shown). Briefly, our extensive ensemble results are insensitive to settings of carbon cycle parameters and the definition of target $\Delta T$. The total $CO_2$-fe emission budget is insensitive to the choice of SSP non-$CO_2$ pathway, although the fractional contributions from $CO_2$ and non-$CO_2$ are. Each test experiment's details and associated results are further described in Text S3 in Supporting Information S1, and the future non-$CO_2$ pathway is discussed in Section 4.

A schematic illustration of the workflow and interaction of the different models is summarized in Figure 1. All AERA scenarios in this study adhere to the relative warming concept, which considers the residual emission amount to achieve the target warming levels relative to the current global warming level in observations (1.2°C in 2020, Terhaar et al., 2022). AERA2.0 and AERA1.5 refer to the 2.0°C and 1.5°C scenarios, respectively. Figure 2 illustrates the emission amount and atmospheric concentration level of $CO_2$ in AERA scenarios compared to those in the SSP1-2.6.

### 2.3. Precipitation Emulation

On climate timescales, latent heat release amount from precipitation is balanced by tropospheric radiative cooling and remaining atmospheric heating caused by various radiative forcing components after considering surface sensible heat flux (Allen & Ingram, 2002; D. Lee et al., 2023; Richardson et al., 2016, 2018; Yeh et al., 2021). To quantify physically decomposed contributions to precipitation change, we use the concept of the decomposable numerical emulation introduced by D. Lee et al. (2023), reproducing the forcing-driven precipitation changes in this climatological atmospheric energy budget sense. These changes can be simplified as functions of temperature and scaled radiative forcings:

$$\Delta \mathrm{P} \sim \alpha \cdot \Delta \mathrm{T} - (\beta/L) \cdot \Delta F_{\mathrm{GHGs}} + (\gamma/L) \cdot \Delta F_{\mathrm{Aerosols}} \quad (1)$$

The $\Delta P$ and $\Delta T$ in Equation 1 represent the annual average globally averaged precipitation and temperature change. $\Delta F_{\mathrm{GHGs}}$ and $\Delta F_{\mathrm{Aerosols}}$ represent the atmospheric radiative energy flux changes caused by greenhouse gases (GHGs) and aerosols. To convert $CO_2$, $CH_4$, and $N_2O$ concentrations into atmospheric radiative forcing amounts ($\Delta F_{\mathrm{CO_2}}$, $\Delta F_{\mathrm{CH_4}}$, and $\Delta F_{\mathrm{N_2O}}$), we utilize the method proposed by Etminan et al. (2016). The effective radiative forcing values of owmGHGs and aerosols under the SSP1-2.6 scenario are adopted from Smith (2020) to estimate $\Delta F_{\mathrm{owmGHGs}}$ and $\Delta F_{\mathrm{Aerosols}}$, respectively. The unit conversion coefficient, denoted as $L$ ($1\%\cdot W^{-1}\cdot m^2$), accounts for the latent heat of condensation (Allen & Ingram, 2002). Three parameters indicate each ensemble's precipitation sensitivities to the temperature ($\alpha$) and the radiative forcings of GHGs ($\beta$) and aerosols ($\gamma$), respectively.

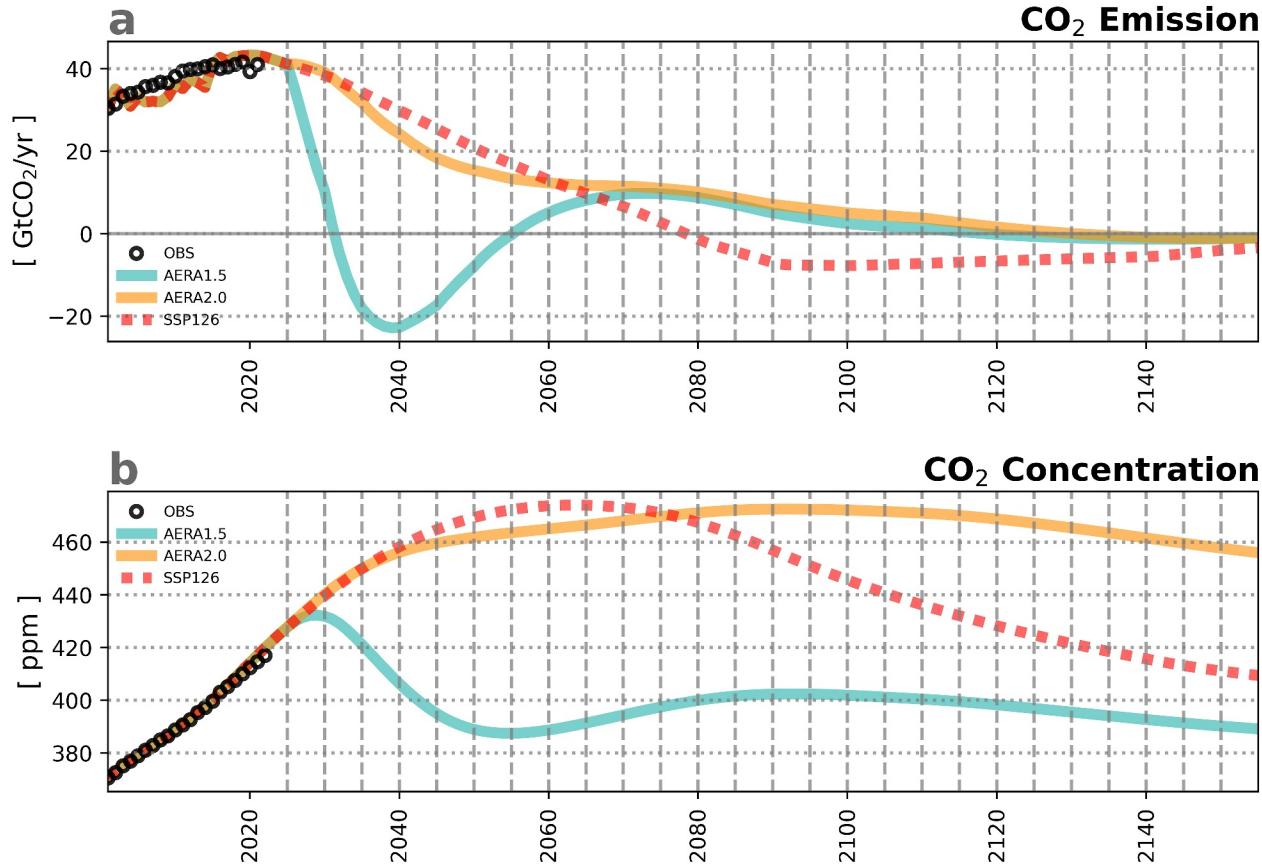


**Figure 2.** (a) Globally averaged annual $CO_2$ emission amount from observations (OBS) and FaIR 5,000 ensemble-averaged results under AERA1.5, AERA2.0, and SSP1-2.6 (SSP126) scenarios, respectively. (b) Same as (a), except for the concentration. (a and b) Vertically dashed lines indicate the stocktake years (every 5 years) from 2025 to 2150, during which the AERA algorithm generates the adjusted scenarios for the next 5 years. Observation data for $CO_2$ emissions and concentrations are taken from Friedlingstein et al. (2022) and Lan et al. (2023) for comparison.

The distinct merit of Equation 1 is conciseness and exemplary performance in reproducing simulated $\Delta P$ (D. Lee et al., 2023; Yeh et al., 2021). As the current version of FaIR does not resolve precipitation variables, we use emulated $\Delta P$ as their simulated results. The three parameters of FaIR are statistically estimated by their relationship with ECS (Watanabe et al., 2018; see process details in Text S4 in Supporting Information S1). To check the validity of the emulated precipitation of FaIR, we compare the FaIR emulated ΔP with the CMIP6 GCMs' simulated $\Delta P$ and confirm their similarities under SSP1-2.6 scenarios (Figure S2 in Supporting Information S1).

The parameters of the HC3F and CLXF ensembles are empirically estimated from their AERA1.5 and AERA2.0 results by considering $CO_2$ forcing differences between two AERA scenarios (see Text S4 in Supporting Information S1). The paired differences between simulated $\Delta P$ and emulated $\Delta P$ of each ensemble member of HC3F and CLXF are mostly within ±0.2% (Figures S3d and S3e in Supporting Information S1), supporting the validity of Equation 1 and estimated parameters in a 20-year-averaged climate sense.

### 2.4. Forcing Contributions to the Emission Budgets and Climate Changes

Our results for $CO_2$-fe emission and changes in $\Delta T$ and $\Delta P$ are decomposed into the anthropogenic contributions from $CO_2$ and non-$CO_2$ components. Since the $CO_2$-fe emissions are computed from FaIR, we run FaIR experiments with individual or combined forcings in AERA scenarios ($CO_2$, non-$CO_2$, $CH_4$, $N_2O$, and aerosols) to explore each forcing contribution to the $CO_2$-fe emission budget. For the contribution of Other forcings (Other), we measure it as the residual after subtracting $CH_4$, $N_2O$, and aerosols from the results of non-$CO_2$, implying the sum of the effects of owmGHGs and other anthropogenic forcings such as land use change, black carbon on snow, aviation contrails which are included in FaIR (Leach et al., 2021). While $CO_2$-fe emission of non-$CO_2$

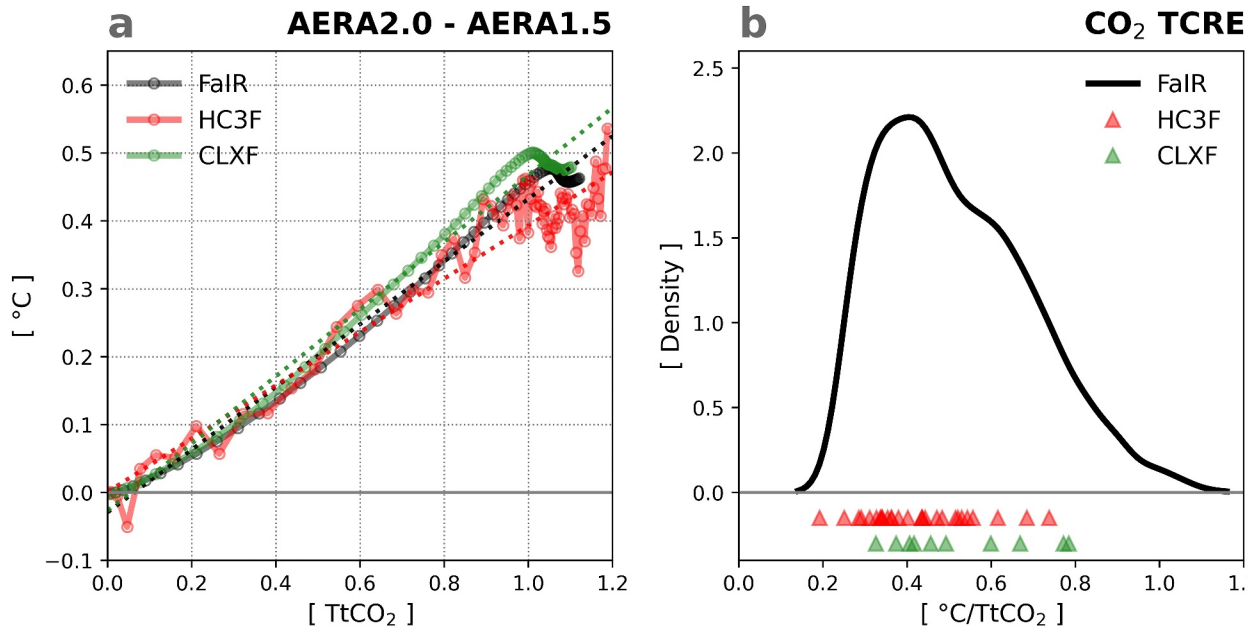


**Figure 3.** (a) Scatter plot for the cumulative emission amount of $CO_2$ and $CO_2$-induced temperature change estimated from the difference between AERA2.0 and AERA1.5, shown in each model ensemble-averaged results. Dotted lines represent the linearly fitted equations for each group according to their TCRE values. (b) The TCRE probability density function from Gaussian kernel density estimation of 5,000 FaIR ensembles. Colored triangles show the TCRE values of each ensemble case of HC3F (red) and CLXF (green), respectively.

components is estimated from the SSP1-2.6 scenario, $CO_2$ emissions are measured individually for AERA1.5 and AERA2.0, respectively.

Accordingly, we collect individual forcing experiment results of FaIR $\Delta T$ to measure each contribution independently. For FaIR, HC3F, and CLXF, we indirectly compute the $CO_2$ and non-$CO_2$ contributions by considering the models' $CO_2$ TCRE sensitivities (Figure 3). This $CO_2$ TCRE value is calculated from the differences in results between AERA2.0 and AERA1.5, where the only difference in their experimental designs is $CO_2$ concentration. By multiplying the cumulative emission of $CO_2$ ($E_{CO_2}$) by TCRE, we estimate the $CO_2$ contribution to $\Delta T$ ($\Delta T_{CO_2}$ in Equation 2). The non-$CO_2$ contribution is estimated by subtracting the $CO_2$ contribution from the gross mean temperature change ($\Delta T_{non-CO_2}$ in Equation 3).

$$\Delta T_{CO_2} \sim \mathrm{TCRE} \cdot E_{CO_2} \tag{2}$$

$$\Delta T_{non-CO_2} \sim \Delta \mathrm{T} - \Delta T_{CO_2} \tag{3}$$

We also examine the forcing contributions to $\Delta P$ based on Equation 1 and $\Delta T$ decomposition (Equations 2 and 3). $CO_2$ and non-$CO_2$ contributions to $\Delta P$ ($\Delta P_{CO_2}$ and $\Delta P_{non-CO_2}$) are calculated by Equations 4 and 5, respectively.

$$\Delta P_{CO_2} = \alpha \cdot \Delta T_{CO_2} - (\beta / L) \cdot \Delta F_{CO_2} \tag{4}$$

$$\Delta P_{non-CO_2} \sim \Delta \mathrm{P} - \Delta P_{CO_2} \tag{5}$$

$\Delta T_{non-CO_2}$ (Equation 3) and $\Delta P_{non-CO_2}$ (Equation 5) of AERA2.0 and AERA1.5 have minimal variations of up to 0.1°C and 0.2% in absolute magnitude, respectively (one standard deviation range from 5,000 FaIR ensembles). These variations originate from the nonlinearity in the radiative forcing interactions between the concentrations of $CO_2$ and non-$CO_2$ GHGs (e.g., Etminan et al., 2016). For simplicity, our non-$CO_2$ results from Equations 3 and 5 only show the averaged results between AERA2.0 and AERA1.5. These TCRE-based contribution sizes are named as statistically estimated quantifications.

In addition to this statistical quantification, we examine the results of FaIR ensembles forced by single forcing components of AERA scenarios, named physically estimated contribution. As we use the emulation for FaIR ΔP (see Section 2.3 and Text S4 in Supporting Information S1), each $CO_2$ and non-$CO_2$ forcing-driven $\Delta P$ can be described as the sum of ΔT effects and fast response to the radiative forcing perturbation effects, as per Equations 4 and 6–9, respectively, by considering the $\Delta T$ decomposition in Equation 10.

$$\Delta P_{CH_4} \sim \alpha \cdot \Delta T_{CH_4} - (\beta/L) \cdot \Delta F_{CH_4} \quad (6)$$

$$\Delta P_{N_2O} \sim \alpha \cdot \Delta T_{N_2O} - (\beta/L) \cdot \Delta F_{N_2O} \quad (7)$$

$$\Delta P_{Other} \sim \alpha \cdot \Delta T_{Other} - (\beta/L) \cdot \Delta F_{owmGHGs} \quad (8)$$

$$\Delta P_{Aerosols} \sim \alpha \cdot \Delta T_{Aerosols} + (\gamma/L) \cdot \Delta F_{Aerosols} \quad (9)$$

$$\Delta T \sim \Delta T_{CO_2} + \Delta T_{CH_4} + \Delta T_{N_2O} + \Delta T_{Other} + \Delta T_{Aerosols} \quad (10)$$

Since the quantified contributions from statistical and physical methods are comparable for both $CO_2$ and non-$CO_2$ cases, we assert the feasibility of TCRE-based statistical estimation (Figures 4c and 5c). Natural forcings, like volcanic and solar forcings, are not considered in our decomposition due to their negligible impacts (about −0.04°C in 2100 from FaIR ensembles) relative to those of anthropogenic forcings (e.g., Lurton et al., 2020; Nazarenko et al., 2022; Terhaar et al., 2022).

### 2.5. $CO_2$ Mitigation Effect Samples

As the forcing difference between the two AERA scenarios is only the $CO_2$ emission amount (Terhaar et al., 2022), we examine the paired-ensemble differences between these scenarios to contrast additional $CO_2$-driven effects on climate. We examine the simulated years of 2026–2100, where AERA splits the mitigation pathways apart from the SSP1-2.6 after the first stocktake year (2025). Since FaIR can only illustrate the global responses, we focus on the results of HC3F and CLXF to highlight the details of the $CO_2$ mitigation effects on regional scales.

To check the robustness of our ESM-like model simulations, we also explore the $CO_2$ mitigation samples from 11 ensembles of CMIP6 ESMs under the scenarios of 1pctCO2 and esm-1pct-brch-1000PgC from the Zero Emissions Commitment Model Intercomparison Project (ZECMIP) introduced by Jones et al. (2019). The esm-1pct-brch-1000PgC scenario sets $CO_2$ emissions to zero after reaching 1,000 PgC (~3.7 $TtCO_2$) cumulative carbon emissions from pre-industrial levels, corresponding to around 2.0°C warming above pre-industrial levels (Jones et al., 2019). The details of the $CO_2$ mitigation sampling process from these CMIP6 ensembles are described in Text S5 in Supporting Information S1. We refer to these samples as CMIP6 (ZECMIP).

As the $CO_2$ concentration is the only difference in CMIP6 (ZECMIP) samples (Figure S4 in Supporting Information S1), their results are similar to the differences between AERA2.0 and AERA1.5 of HC3F and CLXF (Figure 6 and Figure S7 in Supporting Information S1). Notably, our results are computed by AERA2.0 minus AERA1.5 (1pctCO2 minus esm-1pct-brch-1000PgC), highlighting the impacts of reduced $CO_2$ mitigation.

## 3. Results

### 3.1. Residual Emission Budget for the Paris Agreement

We examine the residual $CO_2$-fe emission budget required to achieve the global warming levels set by the Paris Agreement. The FaIR results of $CO_2$ emissions and concentrations align well with observations for the recent period (Figure 2). AERA suggests that emissions should decrease to near zero for the late 21st century (Figure 2 and Figure S1 in Supporting Information S1), resulting in a gradual decline in $CO_2$ concentration beyond the simulation year 2100 (Figure 2). To quantify the residual emission budget, we cumulate the $CO_2$-fe emission amount from 2021 to 2100 (Figure 4). The cumulative emission amount increases gradually in the middle of the 21st century for all AERA scenarios. However, its trend progressively decreases and reaches near zero around 2100 for AERA1.5 and 2120 for AERA2.0 (Figures 2a and 4a and Figure S5a in Supporting Information S1).

10.1029/2024EF005580



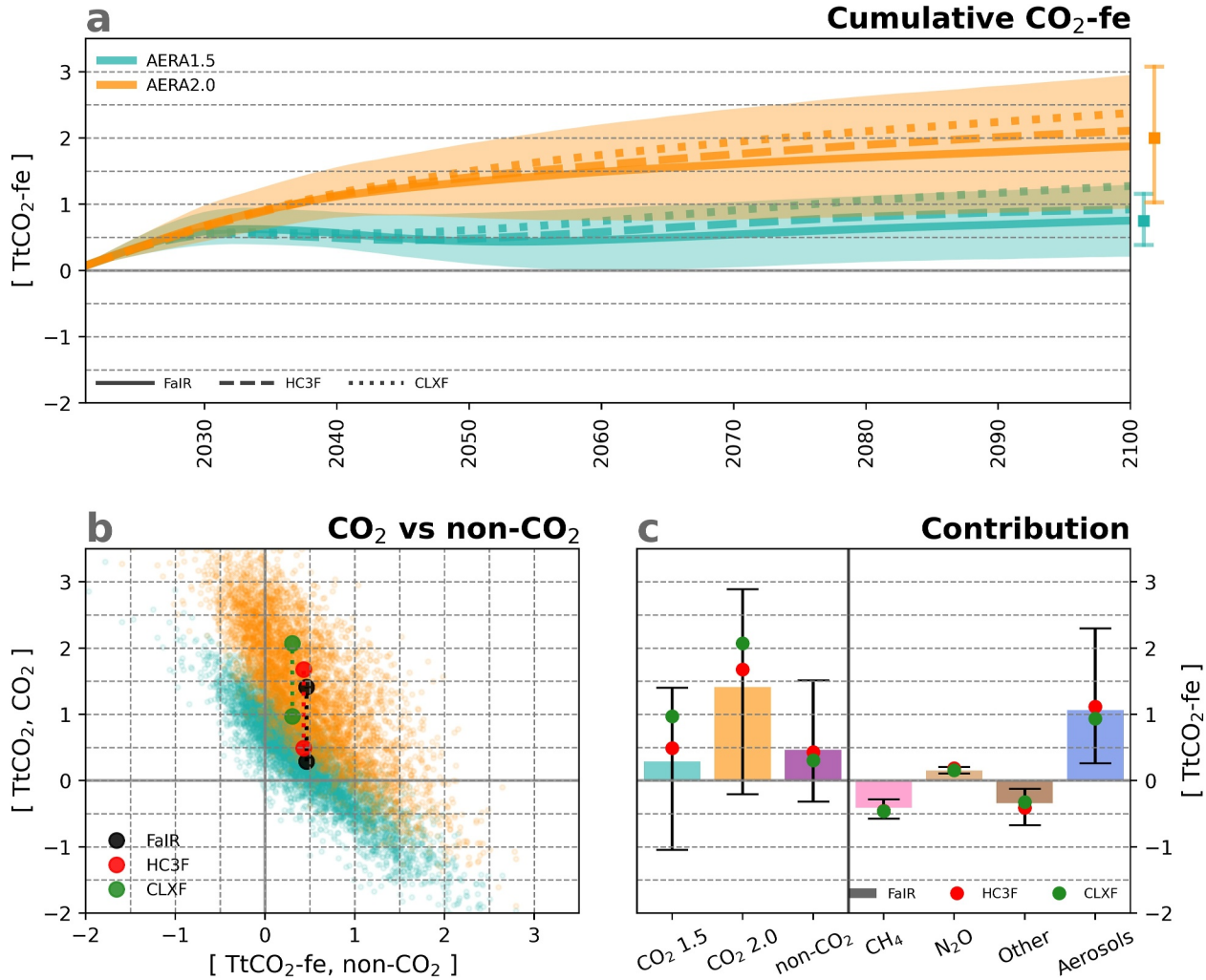


**Figure 4.** (a) Time series of cumulative $CO_2$-fe emission amounts since 2021 under the 1.5°C (AERA1.5) and 2.0°C (AERA2.0) scenarios. The ensemble-averaged values are shown by thick solid, dashed, and dotted lines for FaIR, HC3F, and CLXF, respectively. For comparison, the observation-constrained $CO_2$-fe TCRE (Jenkins et al., 2021) based budgets for 1.5°C and 2.0°C warming levels are displayed with error bars (90% confidence intervals) and squares (medians). (b) Scatter plots for cumulative emission amount of $CO_2$ and non$CO_2$-fe of FaIR ensembles by the year 2100 under AERA1.5 and AERA2.0 scenarios. The ensemble-averaged values of FaIR, HC3F, and CLXF are denoted in black, red, and green circles. The dotted lines show the $CO_2$ emission mitigation amount for half a degree differences (AERA2.0—AERA1.5). (c) Human-induced $CO_2$-fe contributions for each forcing component of AERA scenarios, measured by FaIR single-forcing experiments. The ensemble-averaged results of HC3F and CLX3F are shown in circles. Shading in (a) and error bars in (c) represent the 5th and 95th percentiles of FaIR ensembles.

In multiple ensembles averaged sense, FaIR converges to a residual emission budget of 0.8 (0.2–1.3 for a 90% confidence interval) and 1.9 (0.9–3.0) $TtCO_2$-fe by 2100 to limit global warming to 1.5°C and 2.0°C, respectively. The ensemble-averaged results of HC3F and CLXF are 0.9 (2.1) and 1.3 (2.4) $TtCO_2$ for AERA1.5 (AERA2.0), which are located within the 90% confidence interval ranges of FaIR. Those results and ensemble spread are similar to the inversely calculated $CO_2$-fe cumulative emission budget from the best observationally constrained $CO_2$-fe TCRE values in Jenkins et al. (2021).

Next, we investigate the $CO_2$-fe budget contributions from $CO_2$ and non-$CO_2$ components by conducting single-forcing experiments with the FaIR models (see Section 2.4). Figure 4b presents the three models' decomposed emission budget amounts under the AERA scenarios. In the FaIR ensemble average, the budget of $CO_2$ emissions is 0.3 and 1.4 $TtCO_2$ for 1.5°C and 2.0°C, while that of non-$CO_2$ is 0.5 $TtCO_2$-fe. A statistically significant (hereinafter: at least 5% significance level) negative correlation is found between the $CO_2$-fe budgets of $CO_2$ and non-$CO_2$ ($r = -0.90$ and $-0.78$ for AERA1.5 and AERA2.0).

10.1029/2024EF005580

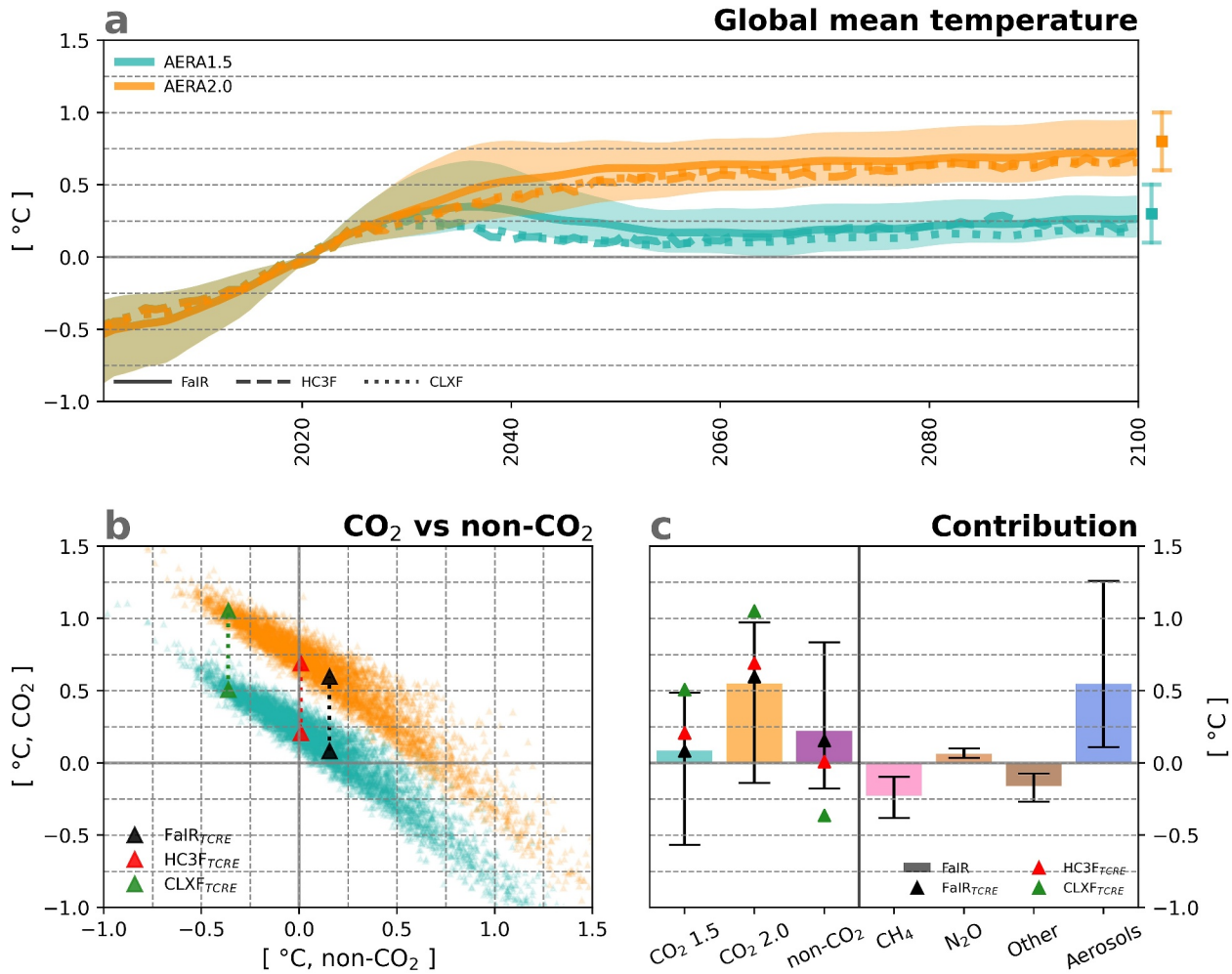


**Figure 5.** (a) Time series of globally averaged surface air temperature relative to the 2011–2030 climate under the 1.5°C (AERA1.5) and 2.0°C (AERA2.0) scenarios. The ensemble-averaged values are shown by thick solid, dashed, and dotted lines for FaIR, HC3F, and CLXF, respectively. For comparison, the likely ranges for the two scenarios are shown by the error bars, representing ±0.2°C around the target warming levels as stated in the AERA algorithm (Terhaar et al., 2022). Squares show the target temperatures of AERA scenarios. (b) The scatter plot illustrates $CO_2$ and non-$CO_2$ forcings contributions to temperature change at 2100, estimated from FaIR ensembles under AERA1.5 and AERA2.0. Black, red, and green triangles denote the ensemble-averaged values of FaIR, HC3F, and CLXF. The quantified contribution size of each group is estimated statistically by TCRE values (see Section 2.4). The dotted lines show the $CO_2$ emission mitigation effects, around 0.5°C, as designed in AERA. (c) Bars and error bars represent the quantified contributions to the temperature change in the year 2100 from the FaIR ensembles under each forcing-only experiment. The triangles represent the ensemble-averaged TCRE-based contribution sizes, corresponding to panel (b). Shading in (a) and error bars in (c) represent the 5th and 95th percentile ranges of the FaIR ensembles.

As AERA non-$CO_2$ emissions are identical, but $CO_2$ emissions differ for all ensemble simulations (see Section 2.2), our findings underscore the critical role of thermal sensitivity to non-$CO_2$ forcings in determining the residual anthropogenic $CO_2$ emissions budget. The ensemble-averaged results of HC3F and CLXF follow the inverse relationship of the FaIR ensemble members, reinforcing the robustness of the relationship between the emission budgets of $CO_2$ and non-$CO_2$ forcers. The budget differences between AERA2.0 and AERA1.5 highlight that reducing future $CO_2$ emissions by around 1.1 Tt$CO_2$ is necessary to achieve half a degree of global warming level mitigation according to the ensemble-averaged results of FaIR, HC3F, and CLXF.

To further analyze the decomposed contributions from non-$CO_2$ components, we examine the results of individual-forcing FaIR simulations (Figure 4c). Following the SSP1-2.6 scenario, the $CO_2$-fe emission amount of $CH_4$ and owmGHGs decreases while $N_2O$ increases slightly (Meinshausen et al., 2020; Smith et al., 2021). Reducing anthropogenic aerosol emissions acts as a positive radiative forcing and, thus, positive $CO_2$-fe emissions. A statistically significant positive relationship is confirmed between aerosols and non-$CO_2$ ($r = 0.95$ from 5,000 FaIR ensemble members, Figure S6a in Supporting Information S1).

10.1029/2024EF005580

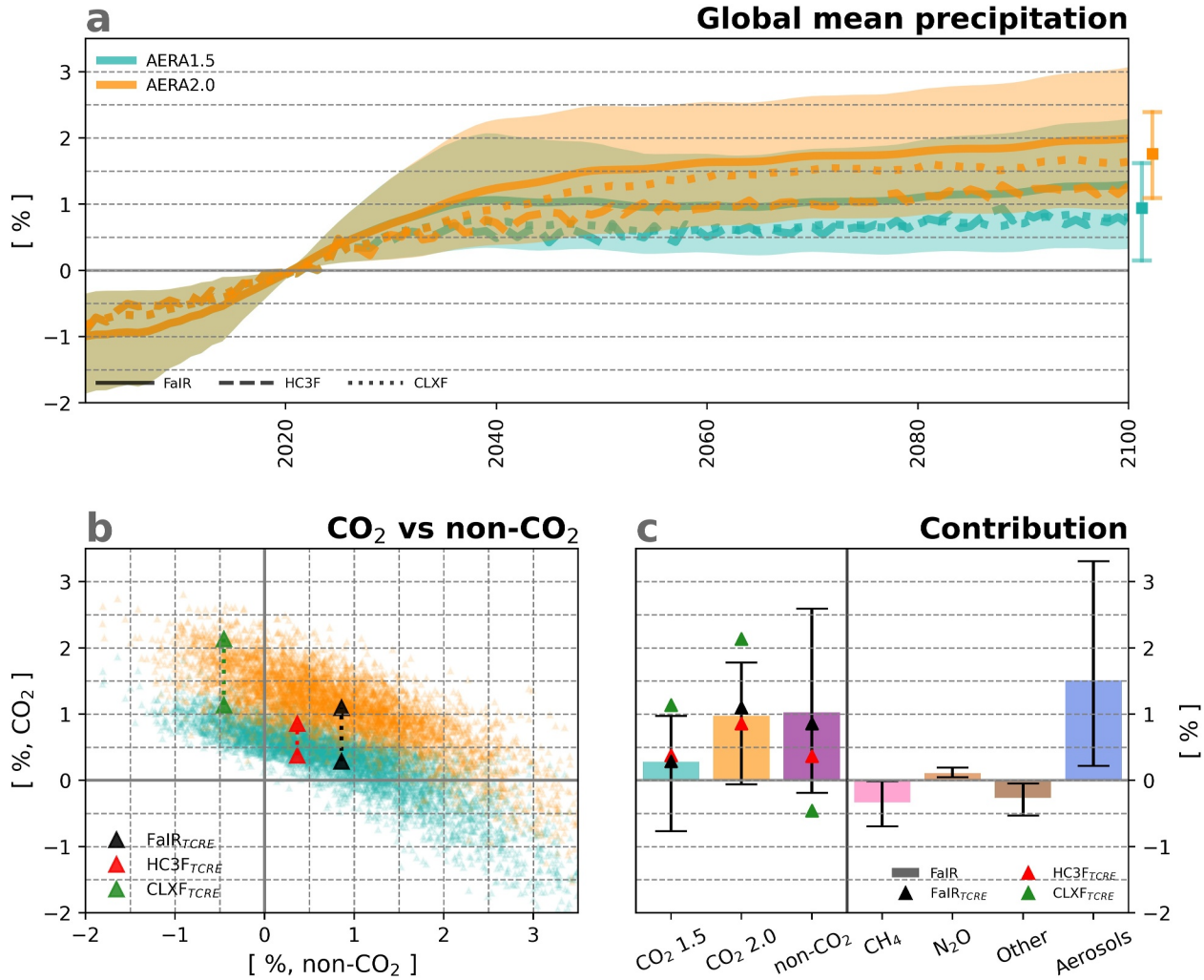


**Figure 6.** Same as Figure 5, except for the globally averaged precipitation change. (a) The likely ranges of the statistical prediction model (D. Lee et al., 2023) are shown together, and squares (error bars) represent the best-estimated values (the 0.5th and 99.5th percentile values) from statistical assumptions based on CMIP6 simulations at two global warming levels of 1.5 and 2.0. (b) $CO_2$ and non-$CO_2$ contributions to precipitation changes in 20-year climate (2081–2100) are statistically estimated using TCRE-based ΔT contribution and the decomposed ΔP emulation equation (see Section 2.4). (c) FaIR single-forcing results of temperature and relevant radiative forcing of GHGs and aerosols are used to estimate the precipitation change (2081–2100) contributions (see Sections 2.3 and 2.4). The triangles represent the ensemble-averaged TCRE-based contribution sizes, corresponding to panel (b). Shading in (a) and error bars in (c) represent the 5th and 95th percentiles of FaIR ensembles.

According to the significant relationships between the budgets of $CO_2$ and non-$CO_2$ and between aerosols and non-$CO_2$, we conclude that the sensitivity in the radiative forcing responses to the aerosols mainly explains the ensemble spread in the emission budget of $CO_2$ and non-$CO_2$. This characteristic is also verified in a statistically significant negative relationship between the budgets of $CO_2$ and aerosols (not shown, $r = -0.84$ and $-0.73$ from 5,000 FaIR ensembles for AERA1.5 and AERA2.0). Primarily, our findings emphasize the importance of assessing the plausible range of aerosol sensitivity, which is key to tackling the considerable uncertainty remaining in the $CO_2$ emission budget.

### 3.2. Forcing-Driven Contribution to Climate Change Under the Paris Agreement

We investigate $\Delta T$ and $\Delta P$ under the AERA scenarios to quantify each forcing-driven contribution to warmer worlds of the Paris Agreement. Our results show the changes relative to the 20-year averaged climate centered on 2020 (2011–2030), conceptually matching with the reference global warming levels in the AERA algorithm (+1.2°C in 2020).

Figure 5 illustrates ΔT under two different mitigation pathways. While the FaIR simulations of SSP1-2.6 exhibit an uncertainty range of 1.4°C between the 5th and 95th percentile values in the year 2100 (not shown), Figure 5a demonstrates that AERA achieves well-centered $\Delta T$ around each target with a much-reduced uncertainty size by incorporating the sensitivities of models (Table 1) into the mitigation future scenarios (Figure 4a). As our AERA experiments use the relative warming framework (see Section 2.2), those ensemble simulation results of $\Delta T$ gradually stabilized around +0.3°C and +0.8°C. The uncertainty size in $\Delta T$ is more considerable for the 2030s than for the later periods of the 21st century because the AERA algorithm effectively shrinks $\Delta T$ uncertainty by controlling $CO_2$ emissions.

To quantify the contributions of $CO_2$ and non-$CO_2$ forcings, we utilize the linear-like characteristic in TCRE (see Section 2.4). In an ensemble-averaged sense, FaIR, HC3F, and CLXF project 0.3°C and 0.8°C of warming in the late 21st century (Figure 5a). The TCRE-based quantification reveals 0.1°C and 0.6°C from $\Delta T_{CO_2}$ for AERA1.5 and AERA2.0, respectively, and 0.2°C from $\Delta T_{non-CO_2}$. Those results are almost equal to the individual forcing experiment results of FaIR $\Delta T_{CO_2}$ (0.1°C and 0.6°C for AERA1.5 and AERA2.0, respectively) and $\Delta T_{non-CO_2}$ (0.2°C), rounded to the first decimal place.

Figure 5b confirms a significant anti-correlation between the $\Delta T_{CO_2}$ and $\Delta T_{non-CO_2}$, consistent with our findings from the residual emission budget analysis (Figure 4b). While the $CO_2$ and non-$CO_2$ contributions from FaIR and HC3F are similar, CLXF exhibits a substantial negative contribution from non-$CO_2$, equivalent to the 5$^{th}$ percentile of the 5,000 FaIR ensembles (Figure S6b in Supporting Information S1). Nonetheless, the various ensembles agree on a half-degree temperature change resulting from the $CO_2$ difference between AERA2.0 and AERA1.5.

The non-$CO_2$ contributions are further decomposed using individual forcing experiments with the FaIR model (Figure 5c). The spread in the non-$CO_2$ contributions is primarily explained by aerosols ($r = 0.93$ from 5,000 FaIR ensembles, Figure S6b in Supporting Information S1). Furthermore, aerosols make up the largest contribution to the response in AERA1.5 (and second-largest in AERA2.0), with 72.1% (40.7%) of the 5,000 ensemble members showing a more considerable contribution to temperature from aerosols than from $CO_2$ in AERA1.5 (AERA2.0).

$\Delta P$ under the two mitigation pathways is illustrated in Figure 6. Figure 6a illustrates the time series of $\Delta P$ from emulations (FaIR, see Section 2.3) and simulations (HC3F and CLXF). The ensemble-averaged time series between the two scenarios are similar between 2025 and 2030s. $\Delta P$ under the two scenarios are split after the 2040s when $\Delta T$ also emerges. Although $\Delta T$ of FaIR, HC3F, and CLXF are similar, they have various $\Delta P$ at either AERA1.5 (+1.2%, +0.8%, and +0.8%) and AERA2.0 (+1.9%, +1.2%, and +1.6%), respectively, because they have different sensitivity in precipitation parameters (Figures S3a–S3c in Supporting Information S1). Regardless of increasing uncertainty sources, our results are primarily within the statistically estimated ranges from CMIP6 simulations (D. Lee et al., 2023), reaffirming the validity of our multi-model extensive ensemble results.

Out of three types of models, HC3F exhibits the smallest $\Delta P$ under AERA2.0 due to its lowest value in the $\alpha$ parameter, representing hydrological sensitivity and indicating how $\Delta P$ scales with $\Delta T$ (Table 1 and Figure S3a in Supporting Information S1). Although AERA2.0 projects ~0.5°C warmer conditions than AERA1.5 (Figure 5a), some ensemble cases of CLXF and FaIR under AERA1.5 have more considerable $\Delta P$ increase than those of HC3F under AERA2.0. Contrary to the good agreement in $\Delta T$ (Figure 5a), this result highlights that $\Delta P$ is more uncertain than $\Delta T$, linked to diverse precipitation sensitivities among the model (Equation 1, Table 1 and Figure S3 in Supporting Information S1).

It is also worth mentioning that the total change in precipitation per degree of warming, that is, the apparent hydrological sensitivity (Fläschner et al., 2016), of AERA1.5 (e.g., 4%/°C, 2.7%/°C, and 2.7%/°C for FaIR, HC3F, and CLXF) is much higher than that of AERA 2.0 (e.g., 2.4%/°C, 1.5%/°C, and 2.0%/°C) because the increased amount of atmospheric $CO_2$ concentration in AERA2.0 inhibits latent heat release and decreases $\Delta P$ effectiveness (Equations 1 and 4).

We decompose the $CO_2$ and non-$CO_2$ contributions to $\Delta P$ ($\Delta P_{CO_2}$ & $\Delta P_{nonCO_2}$) as described in Section 2.4 (Figure 6b). The forcing-induced contribution to $\Delta P$ is shown as a 20-year average (2081–2100) to minimize uncertainty from interannual variability. In the FaIR ensemble average, the TCRE-based statistical quantification reveals that $CO_2$ contributes 0.3% and 1.1% to ΔP in AERA1.5 and AERA2.0, respectively, and nonCO$_2$

contributes 0.9%. Those results are close to the individual forcing experiment results of FaIR (0.3%, 1.0%, and 1.0% for AERA1.5 $\Delta P_{CO_2}$, AERA2.0 $\Delta P_{CO_2}$, and $\Delta P_{non-CO_2}$).

We also confirm a significant anti-correlation between $\Delta P_{CO_2}$ and $\Delta P_{nonCO_2}$, consistent with the results obtained from the analysis of the emission budget and $\Delta T$ (Figures 4b and 5b). The TCRE-based $CO_2$ mitigation effects for half a degree (Figure 6b: 0.8%, 0.5%, and 1.0% for FaIR, HC3, and CLXF) are similar to $\Delta P$ differences between AERA2.0 and AERA1.5 (Figure 6a: 0.7%, 0.4%, and, 0.8% for FaIR, HC3, and CLXF), reaffirming the validity of linear assumptions in the calculation (e.g., Figures 3a and 5c).

In Figure 6c, the spread in $\Delta P_{non-CO_2}$ is explained primarily by $\Delta P_{Aerosols}$ ($r = 0.94$ from 5,000 FaIR ensemble members, Figure S6c in Supporting Information S1). Remarkably, both the contribution sizes and the uncertainties from aerosols are the largest out of all anthropogenic forcings, implying again the critical role of anthropogenic aerosols in driving $\Delta P$ at 1.5°C and 2.0°C stabilized worlds. Additionally, 81.0% (59.0%) of 5,000 ensemble members reveal a greater contribution to $\Delta P$ from aerosols than from $CO_2$ in AERA1.5 (AERA2.0), stressing the necessity of better quantifying aerosol impacts.

### 3.3. $CO_2$ Mitigation Effects on the Hydrological Cycle

In our $CO_2$-controlled simulations, inter-model uncertainty is more remarkable in $\Delta P$ than $\Delta T$ (Figure 6a), originating from diversity in precipitation sensitivities. To isolate the uncertainties from the non-$CO_2$ contributions and address the significance of $CO_2$ mitigation effects, we investigate the paired differences between AERA2.0 and AERA1.5 to disclose the specific response from adding $CO_2$ at different $CO_2$-induced global warming levels ($\Delta T_{CO_2}$). Since FaIR results are not spatially resolved, CMIP6 (ZECMIP) samples are additionally examined (see Section 2.5 and Text S5 in Supporting Information S1). The paired differences between simulations at different $CO_2$ concentrations identically display the additional $CO_2$ emission effects, showing the inverse of $CO_2$ mitigation effects (Figure 7 and Figure S7 in Supporting Information S1).

As the impacts of $CO_2$ radiative forcing on regional temperature are clear (Figures 5 and 6, and Figure S7 in Supporting Information S1), we focus on examining the $CO_2$-induced hydrological cycle shift. Since HC3F has the most ensembles except FaIR, we draw a probability density function (PDF) for each bin of global warming levels from its ensembles. These PDF results, computed by Gaussian kernel density estimation, illustrate the chance of experiencing a shifted climate at the global warming levels caused by additional $CO_2$ emissions.

Temperatures rise worldwide (Figures S7a–S7c in Supporting Information S1), but regional precipitation changes are highly inhomogeneous: wet and dry patterns (Figures S7d–S7f in Supporting Information S1) under the addition of $CO_2$. Contrary to the immense uncertainties in $\Delta P_{non-CO_2}$ (Figure 6c and Figure S6c in Supporting Information S1), we find robust model agreements in the global and some regional $CO_2$-induced precipitation changes (Figure 7a and Figures S7d–S7f in Supporting Information S1).

In terms of globally averaged responses, $\Delta P_{CO_2}$ (Figure 7b), the samples of HC3F, CLXF, and CMIP6 (ZECMIP) indicate larger $\Delta P_{CO_2}$ at the warmer $\Delta T_{CO_2}$, highlighting the dominant effects of $\Delta T_{CO_2}$ increases rather than offsetting effects from $CO_2$ radiative heating (Equation 4). Specifically, CLXF exhibits the most extensive changes, reflecting its higher $\alpha$ value than for other models (Figure S3a in Supporting Information S1). The probability of a positive $\Delta P_{CO_2}$ exceeds 92.0% from the bins warmer than 0.2°C $\Delta T_{CO2}$ (Figure 7b), showing that for our large ensemble size, even a tiny warming increment can shift the $\Delta P$ to a new standard, frequently experiencing a wetter year than the current state.

We identify six "hotspot" regions having statistically significant precipitation change at $\Delta T_{CO_2}$ levels of 0.5°C. Among the wet-hotspot regions, the Arctic and Antarctic show a clear signal of precipitation increase, with less than a 10% chance of a dry climate within the 0.2°C–0.6°C warming bins (Figures 7c and 7f). This likelihood implies a clear benefit of $CO_2$ mitigation in these regions, preventing rapid hydrological climate shifts. The equatorial Pacific and Asia regions also demonstrate consistent precipitation increases, with their PDFs transitioning to positive values in all climate model groups (Figures 7d and 7e).

The two dry regions (Atlantic and southeastern Pacific) are likely to experience a drier climate with increasing atmospheric $CO_2$. The probability of a climate shift in dry hotspot regions is smaller than in wet hotspot regions (Figures 7g and 7h). These drying patterns suggest the presence of dynamical processes that outweigh the positive

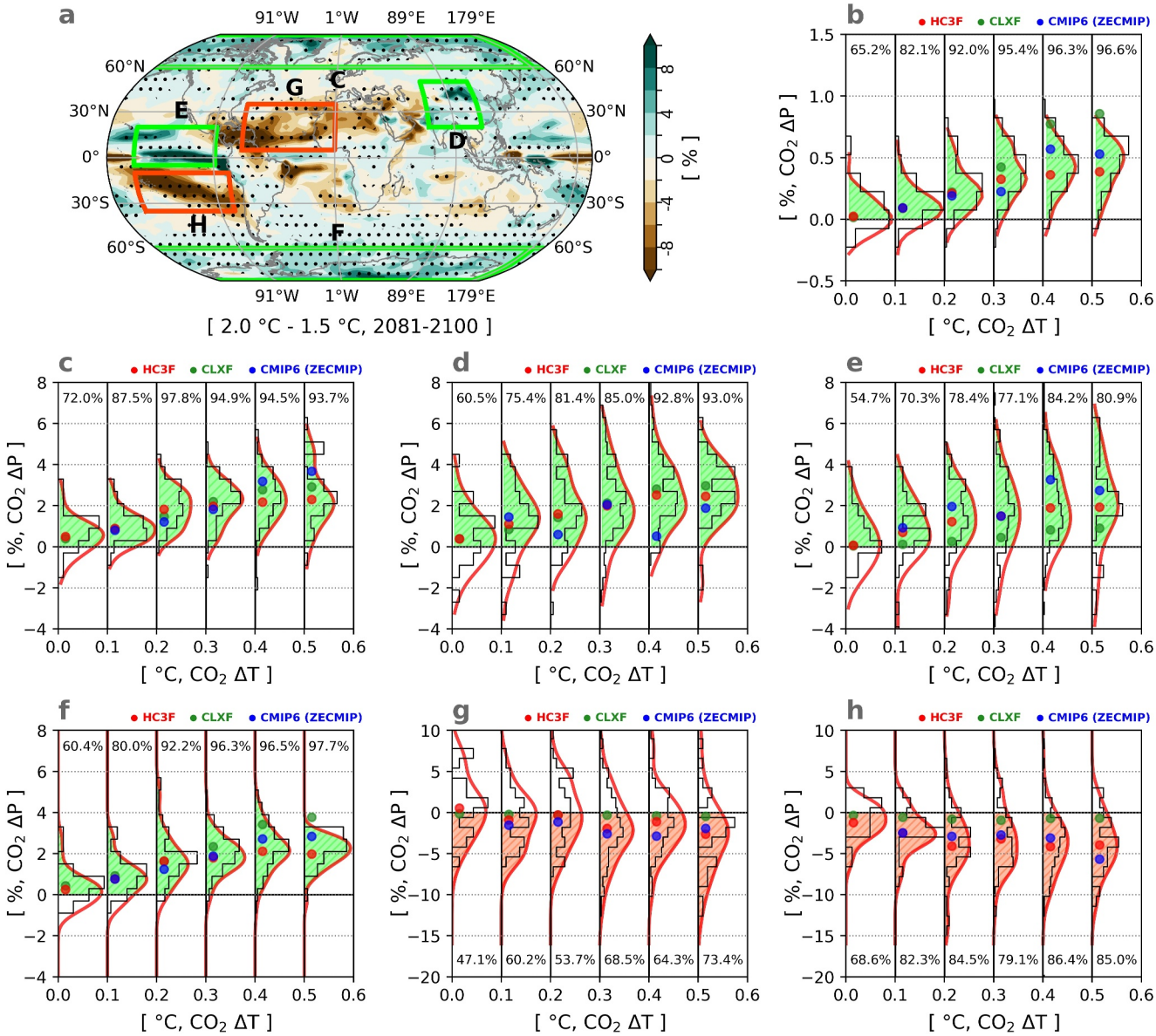


**Figure 7.** (a) Additional $CO_2$ emission effects on precipitation change at around 0.5°C additional global warming by measuring 20 years (2081–2100) climate change difference between HC3F AERA2.0 and HC3F AERA1.5 relative to 2011–2030. Stipples in grids indicate statistically significant differences at the 5% significance level based on the paired *t*-test. Boxes denote the hot spot regions with two colors: green (wet) and orange (dry). (b) Probability density function (PDF) of globally averaged precipitation samples, grouped by six bins of the global warming levels. For PDF, gaussian kernel density estimation is applied for 20 years of climate difference of HC3F, which are collected from 2021 to 2100 for every 5-year shift. The raw histograms of HC3F samples are shown together with solid black lines for comparison. The samples of CLXF and CMIP6 (ZECMIP) only show the sample-averaged results for comparison with those of HC3F (circles). The positive climate shift probability in the PDF is shaded with green colors, and these numbers are shown together. (c–f) Same as (b), except for the four wet regions. (g and h) Same as (b–f) except for the two dry regions emphasizing the negative climate shift probability in the PDF with orange colors.

thermodynamic contribution from rising temperature effects, leading to more water vapor in the atmosphere (Figures S7a–S7c in Supporting Information S1).

We highlight the significance of our finding that, despite the large variations in climate model sensitivities (Table 1 and Figure S3 in Supporting Information S1) and disagreement in the contribution signs of non-$CO_2$ forcings (Figure 6c), all model results agree on the sign of global-mean changes (Figure 7b) and in hotspot regions (Figures 7c–7f) caused by additional $CO_2$ emissions. This consensus supports the understanding that reducing $CO_2$ emissions can robustly alter the magnitude of changes in temperature and precipitation (Figure S7 in Supporting Information S1).

## 4. Discussion and Conclusions

This study aims to provide a physically based estimate of the range of radiative forcing contributions compatible with the 1.5°C and 2.0°C global warming targets, as well as the corresponding impacts on temperature and precipitation at global and regional scales. To achieve this, we exploit a set of perturbed-physics multi-ensemble simulations from three types of ESM-like climate models with a range of thermal, carbon, and hydrological sensitivities, forced with adaptive emission scenarios for 1.5°C and 2.0°C.

Our study fills a gap in the existing literature of ESM-based or emulator-based research exploring various mitigation scenarios pursuing the goals of the Paris Agreement. Studies based on ESMs typically use small ensemble sizes (e.g., Silvy et al., 2024), limiting their ability to assess structural model uncertainty. Those based on simple emulators have large ensemble sizes (e.g., Jenkins et al., 2021; Lamboll et al., 2023; Watson-Parris & Smith, 2022). However, these scenarios must be verified and compared with results from ESMs. Our study introduces a new method to run ESM-like hybrid models (HC3F & CLXF) considering carbon cycle interactions in the globally averaged sense, which demand much less computing cost than ESM.

We manifest that the 1.5°C and 2.0°C samples of AERA are physically and politically the best projections to analyze the impacts under the factual mitigation plan of UNFCCC, given the shortcomings of preexisting samples: mismatched net-zero concept, decreasing $CO_2$ emissions (Meinshausen et al., 2011, 2020); neglected interaction between atmosphere and ocean (Lo et al., 2019; Mitchell et al., 2017), limiting realism in the simulation of the climatological mean and extreme phenomena (Chu et al., 2020; Fischer et al., 2018; Huang et al., 2022; King et al., 2018); or using single GCMs in an empirical mitigation pathway (Graff et al., 2019; Sanderson et al., 2017; Sigmond et al., 2018).

Our $CO_2$ residual emission budgets (0.3 $TtCO_2$ and 1.4 $TtCO_2$ for 1.5°C and 2.0°C) agree well with previously suggested values (Dickau et al., 2022; Jenkins et al., 2021; Matthews et al., 2020; Nicholls et al., 2020). While existing CMIP projections have broad ranges of $\Delta T$ uncertainty due to diverse sensitivities to given identical forcings (e.g., Tebaldi et al., 2021), the AERA algorithm successfully stabilizes $\Delta T$ for each model ensemble near the targets of the Paris Agreement by controlling the $CO_2$ emission at every stocktake year.

By design, in our method, the $CO_2$ budget is significantly anti-correlated with the non-$CO_2$ budget, consistent with the offsetting in residual $CO_2$ budgets from non-$CO_2$ components (Jenkins et al., 2021; Lamboll et al., 2023; Mengis & Matthews, 2020). Since our results reveal that $\Delta T_{\mathrm{Aerosols}}$ explains nearly all of the perturbed physics ensemble spread in $\Delta T_{\mathrm{non-CO_2}}$, we highlight that a better understanding of aerosol-induced radiative forcings and thermal response would effectively reduce the uncertainty range of mitigation pathways (e.g., Regayre et al., 2018), and this would be especially urgent if the 1.5°C target is pursued (Sanderson, 2023; Watson-Parris & Smith, 2022).

As $\Delta P$ is made up of temperature-dependent and independent responses (e.g., Allen & Ingram, 2002; Fläschner et al., 2016; D. Lee et al., 2023; Yeh et al., 2021), ensemble spread in precipitation sensitivities (Figures S3a–S3c in Supporting Information S1) considerably increases the projection uncertainties in $\Delta P$ (comparable to $\Delta P$ spread in SSP1-2.6, Figure S2 in Supporting Information S1) relative to $\Delta T$. The emulated and simulated $\Delta P$ at 1.5°C and 2.0°C are within the statistical model estimation based on SSP scenarios (D. Lee et al., 2023). This study is the first to decompose the $\Delta P$ responses at 1.5°C and 2.0°C into contributions from each climate forcing, as shown in previous literature for the $\Delta T$ case (e.g., Jenkins et al., 2021). Our results reaffirm the key influence of aerosols and suggest potential pitfalls of quantifying aerosol impacts from a single model, without accounting for model uncertainty in aerosol sensitivity (e.g., Wang et al., 2023; W. Zhang & Zhou, 2021). Our decomposition method (Equation 4) arithmetically reveals that $\Delta F_{\mathrm{CO_2}}$ offsets positive contributions of $\Delta T$ (D. Lee et al., 2023; Yeh et al., 2021) and explains why the total change in $\Delta P$ per degree of $\Delta T$ under forcing perturbed condition is higher for AERA1.5 than AERA2.0, similar to the results from CMIP5 experiments (Hegerl et al., 2015; Mitchell et al., 2016): it for the lowest $CO_2$ emission scenario, Representative Concentration Pathway 2.6 (RCP2.6), is higher than it for the highest (RCP8.5).

In contrast to the considerable uncertainty in non-$CO_2$ contributions, we highlight the robust and statistically significant $CO_2$ forcing-driven effects on temperature and precipitation at global and regional scales for a relatively modest $CO_2$ increase compatible with 0.5°C extra warming (Figure 7 and Figure S7 in Supporting Information S1). Additional $CO_2$ emissions from AERA1.5 to AERA2.0 induce a climate shift, with regional

warming, wetting, and drying. Our regional precipitation responses to extra $CO_2$ emissions correspond to those of He and Soden (2017) and Douville and John (2021), explaining regional drying patterns by (a) moisture divergence enhanced by land-sea contrasts and sea surface warming patterns and (b) direct radiative forcing of $CO_2$ inhibiting local evaporation. Remarkably, we find that even additional $CO_2$ resulting in just 0.2°C $\Delta T_{CO_2}$ is very likely to provoke a detectable hydrological climate shift for 20-year averages over the globe and in polar regions (Figures 7b, 7c, and 7f), providing essential information for policymakers and stakeholders striving to meet the objectives of the Paris Agreement.

We discuss three potential caveats in this study. First, our HC3F and CLXF AERA experiments cover relatively short simulations (up to year ∼2100), preventing an assessment of the long-term response of the carbon cycle. Since long-term carbon cycle responses may continuously change the climate for decades (e.g., Allen et al., 2022; Jenkins et al., 2022), extended AERA simulations are necessary to explore the pathways beyond net-zero emissions. Second, noteworthily, present-day $CH_4$ and $N_2O$ emissions are continuing to rise (Fletcher & Schaefer, 2019; Forster et al., 2023), suggesting that the empirical pathways of non-$CO_2$ forcers may differ from the values devised in the CMIP6 SSP1-2.6 scenario. Additional adaptive emission experiments must include scenario uncertainties from non-$CO_2$ agents (see Section 2.2, e.g., Cain et al., 2022; Hienola et al., 2018). Lastly, our findings focus on the climatological mean responses but ignore high-impact extreme events (e.g., Farinosi et al., 2020; D. Lee et al., 2024; Seneviratne & Hauser, 2020; X. Zhang et al., 2023). We highlight extreme event analysis in the stabilized global warming conditions under adaptive emission scenarios as a worthwhile avenue for future research.

## Data Availability Statement

The data of FaIR, HadCM3-FaIR (HC3F) and CLIMBER-X-FaIR (CLXF) on which this article is based are available at D. Lee (2024). Observation data sets of $CO_2$ emission and concentration are obtained from Friedlingstein et al. (2022) and Lan et al. (2023). CMIP6 model simulations can be accessed at https://esgf-node.llnl.gov/projects/cmip6/. CMIP6 scenario data sets for emissions & concentrations and effective radiative forcings are obtained from Nicholls and Lewis (2021) and Smith (2020), respectively.

**Acknowledgments**
D.L. and M.R.A. are funded by the European Union's Horizon 2020 research and innovation programme (4C project, Grant 821003). We also acknowledge support by UK Research and Innovation (UKRI) under the UK government's Horizon Europe funding Guarantee, Grant EP/Y036123/1 (P.C.), and by UKRI Natural Environmental Research Council (NERC) Grants NE/V012045/1 (P.C.) and NE/T006250/1 (D.L. and P.C.). M.W. is funded by the German climate modeling project PalMod supported by the German Federal Ministry of Education and Research (BMBF) as a Research for Sustainability initiative (FONA) (Grants 01LP1920B, 01LP1917D and 01LP2305B). We acknowledge the World Climate Research Programme, which, through its Working Group on Coupled Modeling, coordinated and promoted CMIP6. We thank the climate modeling groups for producing and making available their model output, the Earth System Grid Federation (ESGF) for archiving the data and providing access, and the multiple funding agencies who support CMIP6 and ESGF. This work used JASMIN, the UK collaborative data analysis facility.

## References

Allen, M. R., Frame, D. J., Huntingford, C., Jones, C. D., Lowe, J. A., Meinshausen, M., & Meinshausen, N. (2009). Warming caused by cumulative carbon emissions towards the trillionth tonne. *Nature*, *458*(7242), 1163–1166. https://doi.org/10.1038/nature08019

Allen, M. R., Friedlingstein, P., Girardin, C. A. J., Jenkins, S., Malhi, Y., Mitchell-Larson, E., et al. (2022). Net zero: Science, origins, and implications. *Annual Review of Environment and Resources*, *47*(1), 849–887. https://doi.org/10.1146/annurev-environ-112320-105050

Allen, M. R., & Ingram, W. J. (2002). Constraints on future changes in climate and the hydrologic cycle. *Nature*, *419*(6903), 224–232. https://doi.org/10.1038/nature01092

Baker, H. S., Millar, R. J., Karoly, D. J., Beyerle, U., Guillod, B. P., Mitchell, D., et al. (2018). Higher $CO_2$ concentrations increase extreme event risk in a 1.5°C world. *Nature Climate Change*, *8*(7), 604–608. https://doi.org/10.1038/s41558-018-0190-1

Cain, M., Jenkins, S., Allen, M. R., Lynch, J., Frame, D. J., Macey, A. H., & Peters, G. P. (2022). Methane and the Paris Agreement temperature goals. *Philosophical Transactions of the Royal Society A: Mathematical, Physical & Engineering Sciences*, *380*(2215), 20200456. https://doi.org/10.1098/rsta.2020.0456

Català, A. P., & Wyns, A. (2022). The global stocktake: A health check for the Paris Agreement. *The Lancet Planetary Health*, *6*(4), e297–e298. https://doi.org/10.1016/s2542-5196(22)00066-3

Chu, J.-E., Lee, S.-S., Timmermann, A., Wengel, C., Stuecker, M. F., & Yamaguchi, R. (2020). Reduced tropical cyclone densities and ocean effects due to anthropogenic greenhouse warming. *Science Advances*, *6*(51), eabd5109. https://doi.org/10.1126/sciadv.abd5109

Dickau, M., Matthews, H. D., & Tokarska, K. B. (2022). The role of remaining carbon budgets and net-zero $CO_2$ targets in climate mitigation policy. *Current Climate Change Reports*, *8*(4), 91–103. https://doi.org/10.1007/s40641-022-00184-8

Douville, H., & John, A. (2021). Fast adjustment versus slow SST-mediated response of daily precipitation statistics to abrupt 4x$CO_2$. *Climate Dynamics*, *56*(3), 1083–1104. https://doi.org/10.1007/s00382-020-05522-w

Etminan, M., Myhre, G., Highwood, E. J., & Shine, K. P. (2016). Radiative forcing of carbon dioxide, methane, and nitrous oxide: A significant revision of the methane radiative forcing. *Geophysical Research Letters*, *43*(24). https://doi.org/10.1002/2016GL071930

Farinosi, F., Dosio, A., Calliari, E., Seliger, R., Alfieri, L., & Naumann, G. (2020). Will the Paris Agreement protect us from hydro-meteorological extremes? *Environmental Research Letters*, *15*(10), 104037. https://doi.org/10.1088/1748-9326/aba869

Fischer, E. M., Beyerle, U., Schleussner, C. F., King, A. D., & Knutti, R. (2018). Biased estimates of changes in climate extremes from prescribed SST simulations. *Geophysical Research Letters*, *45*(16), 8500–8509. https://doi.org/10.1029/2018GL079176

Fläschner, D., Mauritsen, T., & Stevens, B. (2016). Understanding the intermodel spread in global-mean hydrological sensitivity. *Journal of Climate*, *29*(2), 801–817. https://doi.org/10.1175/JCLI-D-15-0351.1

Fletcher, S. E. M., & Schaefer, H. (2019). Rising methane: A new climate challenge. *Science*, *364*(6444), 932–933. https://doi.org/10.1126/science.aax1828

Forster, P. M., Smith, C. J., Walsh, T., Lamb, W. F., Lamboll, R., Hauser, M., et al. (2023). Indicators of global climate change 2022: Annual update of large-scale indicators of the state of the climate system and human influence. *Earth System Science Data*, *15*(6), 2295–2327. https://doi.org/10.5194/essd-15-2295-2023

Friedlingstein, P., O'Sullivan, M., Jones, M. W., Andrew, R. M., Gregor, L., Hauck, J., et al. (2022). Global carbon budget 2022 [Dataset]. *Earth System Science Data*, *14*(11), 4811–4900. https://doi.org/10.5194/essd-14-4811-2022

Graff, L. S., Iversen, T., Bethke, I., Debernard, J. B., Seland, Ø., Bentsen, M., et al. (2019). Arctic amplification under global warming of 1.5 and 2°C in noresm1-happi. *Earth System Dynamics*, *10*(3), 569–598. https://doi.org/10.5194/esd-10-569-2019

Haustein, K., Allen, M. R., Forster, P. M., Otto, F. E. L., Mitchell, D. M., Matthews, H. D., & Frame, D. J. (2017). A real-time global warming index. *Scientific Reports*, *7*(1), 15417. https://doi.org/10.1038/s41598-017-14828-5

He, J., & Soden, B. J. (2017). A re-examination of the projected subtropical precipitation decline. *Nature Climate Change*, *7*(1), 53–57. https://doi.org/10.1038/nclimate3157

Hegerl, G. C., Black, E., Allan, R. P., Ingram, W. J., Polson, D., Trenberth, K. E., et al. (2015). Challenges in quantifying changes in the global water cycle. *Bulletin of the American Meteorological Society*, *96*(7), 1097–1115. https://doi.org/10.1175/BAMS-D-13-00212.1

Hienola, A., Partanen, A.-I., Pietikäinen, J.-P., O'Donnell, D., Korhonen, H., Matthews, H. D., & Laaksonen, A. (2018). The impact of aerosol emissions on the 1.5°C pathways. *Environmental Research Letters*, *13*(4), 044011. https://doi.org/10.1088/1748-9326/aab1b2

Huang, Y., Wang, Y., & Ziehn, T. (2022). Nonlinear interactions of land carbon cycle feedbacks in Earth System Models. *Global Change Biology*, *28*(1), 296–306. https://doi.org/10.1111/gcb.15953

IPCC. (2013). In T. F. Stocker, D. Qin, G.-K. Plattner, M. Tignor, S. K. Allen, et al. (Eds.), *Climate Change 2013: The Physical Science Basis. Contribution of Working Group I to the Fifth Assessment Report of the Intergovernmental Panel on Climate Change* (p. 1535). Cambridge University Press.

IPCC. (2018). Summary for policymakers. In V. Masson-Delmotte, P. Zhai, H.-O. Pörtner, D. Roberts, J. Skea, et al. (Eds.), *Global Warming of 1.5°C. An IPCC Special Report on the impacts of global warming of 1.5°C above pre-industrial levels and related global greenhouse gas emission pathways, in the context of strengthening the global response to the threat of climate change, sustainable development, and efforts to eradicate poverty* (pp. 3–24). Cambridge University Press. https://doi.org/10.1017/9781009157940.001

Jahn, A. (2018). Reduced probability of ice-free summers for 1.5°C compared to 2°C warming. *Nature Climate Change*, *8*(5), 409–413. https://doi.org/10.1038/s41558-018-0127-8

Jenkins, S., Cain, M., Friedlingstein, P., Gillett, N., Walsh, T., & Allen, M. R. (2021). Quantifying non-$CO_2$ contributions to remaining carbon budgets. *Npj Climate and Atmospheric Science*, *4*(1), 47. https://doi.org/10.1038/s41612-021-00203-9

Jenkins, S., Millar, R. J., Leach, N., & Allen, M. R. (2018). Framing climate goals in terms of cumulative $CO_2$-forcing-equivalent emissions. *Geophysical Research Letters*, *45*(6), 2795–2804. https://doi.org/10.1002/2017GL076173

Jenkins, S., Sanderson, B., Peters, G., Frölicher, T. L., Friedlingstein, P., & Allen, M. (2022). The multi-decadal response to net zero $CO_2$ emissions and implications for emissions policy. *Geophysical Research Letters*, *49*(23). https://doi.org/10.1029/2022GL101047

Jones, C. D., & Friedlingstein, P. (2020). Quantifying process-level uncertainty contributions to TCRE and carbon budgets for meeting Paris Agreement climate targets. *Environmental Research Letters*, *15*(7), 074019. https://doi.org/10.1088/1748-9326/ab858a

Jones, C. D., Frölicher, T. L., Koven, C., MacDougall, A. H., Matthews, H. D., Zickfeld, K., et al. (2019). The zero emissions commitment model intercomparison project (ZECMIP) contribution to C4MIP: Quantifying committed climate changes following zero carbon emissions. *Geoscientific Model Development*, *12*(10), 4375–4385. https://doi.org/10.5194/gmd-12-4375-2019

King, A. D., Knutti, R., Uhe, P., Mitchell, D. M., Lewis, S. C., Arblaster, J. M., & Freychet, N. (2018). On the linearity of local and regional temperature changes from 1.5°C to 2°C of global warming. *Journal of Climate*, *31*(18), 7495–7514. https://doi.org/10.1175/JCLI-D-17-0649.1

Lamboll, R. D., Nicholls, Z. R., Smith, C. J., Kikstra, J. S., Byers, E., & Rogelj, J. (2023). Assessing the size and uncertainty of remaining carbon budgets. *Nature Climate Change*, *13*(12), 1360–1367. https://doi.org/10.1038/s41558-023-01848-5

Lan, X., Tans, P., Thoning, K., & NOAA Global Monitoring Laboratory. (2023). Trends in globally-averaged $CO_2$ determined from NOAA global monitoring laboratory measurements [Dataset]. *NOAA GML*. https://doi.org/10.15138/9N0H-ZH07

Leach, N. J., Jenkins, S., Nicholls, Z., Smith, C. J., Lynch, J., Cain, M., et al. (2021). FaIRv2. 0.0: A generalized impulse response model for climate uncertainty and future scenario exploration. *Geoscientific Model Development*, *14*(5), 3007–3036. https://doi.org/10.5194/gmd-14-3007-2021

Lee, D. (2024). Quantifying $CO_2$ and non-$CO_2$ contributions to climate change under the adaptive emission scenarios [Dataset]. *Mendeley Data, V1*. https://doi.org/10.17632/7zfgy8zswr.1

Lee, D., Min, S.-K., Fischer, E., Shiogama, H., Bethke, I., Lierhammer, L., & Scinocca, J. F. (2018). Impacts of half a degree additional warming on the Asian summer monsoon rainfall characteristics. *Environmental Research Letters*, *13*(4), 044033. https://doi.org/10.1088/1748-9326/aab55d

Lee, D., Sparrow, S., Leach, N., Osprey, S., Lee, J., & Allen, M. (2024). The attribution of February extremes over North America: A forecast-based storyline study. *Journal of Climate*, *37*(19), 5073–5089. https://doi.org/10.1175/JCLI-D-24-0074.1

Lee, D., Sparrow, S. N., Min, S. K., Yeh, S. W., & Allen, M. R. (2023). Physically based equation representing the forcing-driven precipitation in climate models. *Environmental Research Letters*, *18*(9), 094063. https://doi.org/10.1088/1748-9326/acf50f

Lee, S.-M., & Min, S.-K. (2018). Heat stress changes over East Asia under 1.5° and 2.0°C global warming targets. *Journal of Climate*, *31*(7), 2819–2831. https://doi.org/10.1175/JCLI-D-17-0449.1

Lehner, F., Coats, S., Stocker, T. F., Pendergrass, A. G., Sanderson, B. M., Raible, C. C., & Smerdon, J. E. (2017). Projected drought risk in 1.5°C and 2°C warmer climates. *Geophysical Research Letters*, *44*(14), 7419–7428. https://doi.org/10.1002/2017GL074117

Lo, Y. T. E., Mitchell, D. M., Gasparrini, A., Vicedo-Cabrera, A. M., Ebi, K. L., Frumhoff, P. C., et al. (2019). Increasing mitigation ambition to meet the Paris Agreement's temperature goal avoids substantial heat-related mortality in U.S. cities. *Science Advances*, *5*(6), eaau4373. https://doi.org/10.1126/sciadv.aau4373

Lurton, T., Balkanski, Y., Bastrikov, V., Bekki, S., Bopp, L., Braconnot, P., et al. (2020). Implementation of the CMIP6 forcing data in the IPSL-CM6A-LR model. *Journal of Advances in Modeling Earth Systems*, *12*(4). https://doi.org/10.1029/2019MS001940

Madakumbura, G. D., Kim, H., Utsumi, N., Shiogama, H., Fischer, E. M., Seland, Ø., et al. (2019). Event-to-event intensification of the hydrologic cycle from 1.5°C to a 2°C warmer world. *Scientific Reports*, *9*(1), 3483. https://doi.org/10.1038/s41598-019-39936-2

Matthews, H. D., Tokarska, K. B., Nicholls, Z. R., Rogelj, J., Canadell, J. G., Friedlingstein, P., et al. (2020). Opportunities and challenges in using remaining carbon budgets to guide climate policy. *Nature Geoscience*, *13*(12), 769–779. https://doi.org/10.1038/s41561-020-00663-3

Meehl, G. A., Senior, C. A., Eyring, V., Flato, G., Lamarque, J.-F., Stouffer, R. J., et al. (2020). Context for interpreting equilibrium climate sensitivity and transient climate response from the CMIP6 Earth system models. *Science Advances*, *6*(26), eaba1981. https://doi.org/10.1126/sciadv.aba1981

Meinshausen, M., Nicholls, Z. R. J., Lewis, J., Gidden, M. J., Vogel, E., Freund, M., et al. (2020). The shared socio-economic pathway (SSP) greenhouse gas concentrations and their extensions to 2500. *Geoscientific Model Development*, *13*(8), 3571–3605. https://doi.org/10.5194/gmd-13-3571-2020

Meinshausen, M., Smith, S. J., Calvin, K., Daniel, J. S., Kainuma, M. L., Lamarque, J. F., et al. (2011). The RCP greenhouse gas concentrations and their extensions from 1765 to 2300. *Climatic Change*, *109*(1–2), 213–241. https://doi.org/10.1007/s10584-011-0156-z

Mengis, N., & Matthews, H. D. (2020). Non-$CO_2$ forcing changes will likely decrease the remaining carbon budget for 1.5°C. *NPJ Climate and Atmospheric Science*, *3*(1), 19. https://doi.org/10.1038/s41612-020-0123-3

Millar, R. J., Fuglestvedt, J. S., Friedlingstein, P., Rogelj, J., Grubb, M. J., Matthews, H. D., et al. (2017). Emission budgets and pathways consistent with limiting warming to 1.5°C. *Nature Geoscience*, *10*(10), 741–747. https://doi.org/10.1038/ngeo3031

Mitchell, D., AchutaRao, K., Allen, M., Bethke, I., Beyerle, U., Ciavarella, A., et al. (2017). Half a degree additional warming, prognosis and projected impacts (HAPPI): Background and experimental design. *Geoscientific Model Development*, *10*(2), 571–583. https://doi.org/10.5194/gmd-10-571-2017

Mitchell, D., James, R., Forster, P. M., Betts, R. A., Shiogama, H., & Allen, M. (2016). Realizing the impacts of a 1.5°C warmer world. *Nature Climate Change*, *6*(8), 735–737. https://doi.org/10.1038/nclimate3055

Nazarenko, L. S., Tausnev, N., Russell, G. L., Rind, D., Miller, R. L., Schmidt, G. A., et al. (2022). Future climate change under SSP emission scenarios with GISS-E2.1. *Journal of Advances in Modeling Earth Systems*, *14*(7). https://doi.org/10.1029/2021MS002871

Nicholls, Z., & Lewis, J. (2021). Reduced complexity model intercomparison project (RCMIP) protocol (v5.1.0) [Dataset]. *Zenodo*. https://doi.org/10.5281/zenodo.4589756

Nicholls, Z. R. J., Gieseke, R., Lewis, J., Nauels, A., & Meinshausen, M. (2020). Implications of non-linearities between cumulative $CO_2$ emissions and $CO_2$-induced warming for assessing the remaining carbon budget. *Environmental Research Letters*, *15*(7), 074017. https://doi.org/10.1088/1748-9326/ab83af

Nijsse, F. J. M. M., Cox, P. M., & Williamson, M. S. (2020). Emergent constraints on transient climate response (TCR) and equilibrium climate sensitivity (ECS) from historical warming in CMIP5 and CMIP6 models. *Earth System Dynamics*, *11*(3), 737–750. https://doi.org/10.5194/esd-11-737-2020

Otto, F. E. L., Frame, D. J., Otto, A., & Allen, M. R. (2015). Embracing uncertainty in climate change policy. *Nature Climate Change*, *5*(10), 917–920. https://doi.org/10.1038/nclimate2716

Paris Agreement. (2015). *Report of the Conference of the Parties to the United Nations Framework Convention on Climate Change*. UNFCCC. Retrieved from https://unfccc.int/process-and-meetings/the-paris-agreement

Park, B.-J., Min, S.-K., & Weller, E. (2022). Lengthening of summer season over the Northern Hemisphere under 1.5°C and 2.0°C global warming. *Environmental Research Letters*, *17*(1), 014012. https://doi.org/10.1088/1748-9326/ac3f64

Regayre, L. A., Johnson, J. S., Yoshioka, M., Pringle, K. J., Sexton, D. M. H., Booth, B. B. B., et al. (2018). Aerosol and physical atmosphere model parameters are both important sources of uncertainty in aerosol ERF. *Atmospheric Chemistry and Physics*, *18*(13), 9975–10006. https://doi.org/10.5194/acp-18-9975-2018

Richardson, T. B., Forster, P. M., Andrews, T., Boucher, O., Faluvegi, G., Fläschner, D., et al. (2018). Drivers of precipitation change: An energetic understanding. *Journal of Climate*, *31*(23), 9641–9657. https://doi.org/10.1175/JCLI-D-17-0240.1

Richardson, T. B., Samset, B. H., Andrews, T., Myhre, G., & Forster, P. M. (2016). An assessment of precipitation adjustment and feedback computation methods. *Journal of Geophysical Research: Atmospheres*, *121*(19), 11–608. https://doi.org/10.1002/2016JD025625

Sanderson, B. M. (2023). Estimating vanishing allowable emissions for 1.5°C. *Nature Climate Change*, *13*(12), 1284–1285. https://doi.org/10.1038/s41558-023-01846-7

Sanderson, B. M., Xu, Y., Tebaldi, C., Wehner, M., O'Neill, B., Jahn, A., et al. (2017). Community climate simulations to assess avoided impacts in 1.5 and 2°C futures. *Earth System Dynamics*, *8*(3), 827–847. https://doi.org/10.5194/esd-8-827-2017

Seneviratne, S. I., & Hauser, M. (2020). Regional climate sensitivity of climate extremes in CMIP6 versus CMIP5 multimodel ensembles. *Earth's Future*, *8*(9). https://doi.org/10.1029/2019EF001474

Sigmond, M., Fyfe, J. C., & Swart, N. C. (2018). Ice-free Arctic projections under the Paris Agreement. *Nature Climate Change*, *8*(5), 404–408. https://doi.org/10.1038/s41558-018-0124-y

Silvy, Y., Frölicher, T. L., Terhaar, J., Joos, F., Burger, F. A., Lacroix, F., et al. (2024). AERA-MIP: Emission pathways, remaining budgets and carbon cycle dynamics compatible with 1.5°C and 2°C global warming stabilization. *Earth System Dynamics*, *15*, 1591–1628. https://doi.org/10.5194/esd-15-1591-2024

Smith, C. J. (2020). Effective radiative forcing time series from the shared socioeconomic pathways (v3.0) [Dataset]. *Zenodo*. https://doi.org/10.5281/zenodo.3973015

Smith, C. Harris, G. R., Palmer, M. D., Bellouin, N., Collins, W., Myhre, G., et al. (2021). Energy budget constraints on the time history of aerosol forcing and climate sensitivity. *Journal of Geophysical Research: Atmospheres*, *126*(13). https://doi.org/10.1029/2020JD033622

Sparrow, S., Millar, R. J., Yamazaki, K., Massey, N., Povey, A. C., Bowery, A., et al. (2018). Finding ocean states that are consistent with observations from a perturbed physics parameter ensemble. *Journal of Climate*, *31*(12), 4639–4656. https://doi.org/10.1175/JCLI-D-17-0514.1

Tebaldi, C., Debeire, K., Eyring, V., Fischer, E., Fyfe, J., Friedlingstein, P., et al. (2021). Climate model projections from the scenario model intercomparison project (ScenarioMIP) of CMIP6. *Earth System Dynamics*, *12*(1), 253–293. https://doi.org/10.5194/esd-12-253-2021

Terhaar, J., Frölicher, T. L., Aschwanden, M. T., Friedlingstein, P., & Joos, F. (2022). Adaptive emission reduction approach to reach any global warming target. *Nature Climate Change*, *12*(12), 1136–1142. https://doi.org/10.1038/s41558-022-01537-9

Wang, P., Yang, Y., Xue, D., Ren, L., Tang, J., Leung, L. R., & Liao, H. (2023). Aerosols overtake greenhouse gases causing a warmer climate and more weather extremes toward carbon neutrality. *Nature Communications*, *14*(1), 7257. https://doi.org/10.1038/s41467-023-42891-2

Watanabe, M., Kamae, Y., Shiogama, H., DeAngelis, A. M., & Suzuki, K. (2018). Low clouds link equilibrium climate sensitivity to hydrological sensitivity. *Nature Climate Change*, *8*(10), 901–906. https://doi.org/10.1038/s41558-018-0272-0

Watson-Parris, D., & Smith, C. J. (2022). Large uncertainty in future warming due to aerosol forcing. *Nature Climate Change*, *12*(12), 1111–1113. https://doi.org/10.1038/s41558-022-01516-0

Wehner, M., Stone, D., Mitchell, D., Shiogama, H., Fischer, E., Graff, L. S., et al. (2018). Changes in extremely hot days under stabilized 1.5 and 2.0°C global warming scenarios as simulated by the HAPPI multi-model ensemble. *Earth System Dynamics*, *9*(1), 299–311. https://doi.org/10.5194/esd-9-299-2018

Willeit, M., Ganopolski, A., Robinson, A., & Edwards, N. R. (2022). The Earth system model CLIMBER-X v1.0—Part 1: Climate model description and validation. *Geoscientific Model Development*, *15*(14), 5905–5948. https://doi.org/10.5194/gmd-15-5905-2022

Willeit, M., Ilyina, T., Liu, B., Heinze, C., Perrette, M., Heinemann, M., et al. (2023). The Earth system model CLIMBER-X v1.0—Part 2: The global carbon cycle. *Geoscientific Model Development*, *16*(12), 3501–3534. https://doi.org/10.5194/gmd-16-3501-2023

Yeh, S.-W., Song, S.-Y., Allan, R. P., An, S.-I., & Shin, J. (2021). Contrasting response of hydrological cycle over land and ocean to a changing $CO_2$ pathway. *Npj Climate and Atmospheric Science*, *4*(1), 53. https://doi.org/10.1038/s41612-021-00206-6

Zhang, W., & Zhou, T. (2021). The effect of modeling strategies on assessments of differential warming impacts of 0.5°C. *Earth's Future*, *9*(4). https://doi.org/10.1029/2020EF001640

Zhang, X., Zhou, T., Zhang, W., Ren, L., Jiang, J., Hu, S., et al. (2023). Increased impact of heat domes on 2021-like heat extremes in North America under global warming. *Nature Communications*, *14*(1), 1690. https://doi.org/10.1038/s41467-023-37309-y

## References From the Supporting Information

Collins, M., Tett, S. F. B., & Cooper, C. (2001). The internal climate variability of HadCM3, a version of the Hadley Centre coupled model without flux adjustments. *Climate Dynamics*, *17*(1), 61–81. https://doi.org/10.1007/s003820000094

Meehl, G. A., Covey, C., Delworth, T., Latif, B., McAvaney, M., Mitchell, J. F. B., et al. (2007). The WCRP CMIP3 multi-model dataset: A new era in climate change research. *Bulletin of the American Meteorological Society*, *88*(9), 1383–1394. https://doi.org/10.1175/bams-88-9-1383

Nzotungicimpaye, C. M., MacIsaac, A. J., & Zickfeld, K. (2023). Delaying methane mitigation increases the risk of breaching the 2°C warming limit. *Communications Earth & Environment*, *4*(1), 250. https://doi.org/10.1038/s43247-023-00898-z

Smith, C. J., Al Khourdajie, A., Yang, P., & Folini, D. (2023). Climate uncertainty impacts on optimal mitigation pathways and social cost of carbon. *Environmental Research Letters*, *18*(9), 094024. https://doi.org/10.1088/1748-9326/acedc6

Taylor, K. E., Stouffer, R. J., & Meehl, G. A. (2012). An overview of CMIP5 and the experiment design. *Bulletin of the American Meteorological Society*, *93*(4), 485–498. https://doi.org/10.1175/BAMS-D-11-00094.1

Tett, S. F. B., Gregory, J. M., Freychet, N., Cartis, C., Mineter, M. J., & Roberts, L. (2022). Does model calibration reduce uncertainty in climate projections? *Journal of Climate*, *35*(8), 2585–2602. https://doi.org/10.1175/JCLI-D-21-0434.1

Valdes, P. J., Armstrong, E., Badger, M. P. S., Bradshaw, C. D., Bragg, F., Crucifix, M., et al. (2017). The BRIDGE HadCM3 family of climate models: HadCM3@Bristol v1.0. *Geoscientific Model Development*, *10*(10), 3715–3743. https://doi.org/10.5194/gmd-10-3715-2017